Nitrate postdeposition processes in Svalbard surface snow

Mats Björkman, Carmen P. Vega, Rafael Kühnel, Francesca Spataro, Antonietta Ianniello, Giulio Esposito, Jan Kaiser, Alina Marca, Andy Hodson, Elisabeth Isaksson, et al.

AGU PUBLICATIONS

JGR

Journal of Geophysical Research: Atmospheres

RESEARCH ARTICLE
10.1002/2013JD021234

Key Points:
- NO_3^- deposition and snowpack processes quantified by surface snow sampling
- NO_3^- dry deposition dominates over postdeposition loss in Ny-Ålesund surface snow
- Br decreases while NO_3^- $\delta(^{18}O)$ increases, suggesting tied BrO-NO_x chemistry

Supporting Information:
- Readme
- Figure S1
- Figure S2
- Figure S3

Correspondence to:
M. P. Björkman,
mats.p.bjorkman@gmail.com

Citation:
Björkman, M. P., et al. (2014), Nitrate postdeposition processes in Svalbard surface snow, *J. Geophys. Res. Atmos.*, *119*, 12,953–12,976, doi:10.1002/2013JD021234.

Received 29 NOV 2013
Accepted 15 OCT 2014
Accepted article online 20 OCT 2014
Published online 25 NOV 2014

Nitrate postdeposition processes in Svalbard surface snow

Mats P. Björkman[1,2,3], Carmen P. Vega[4], Rafael Kühnel[1,2], Francesca Spataro[5], Antonietta Ianniello[5], Giulio Esposito[5], Jan Kaiser[6], Alina Marca[6], Andy Hodson[7], Elisabeth Isaksson[1], and Tjarda J. Roberts[8]

[1]Norwegian Polar Institute, Tromsø, Norway, [2]Department of Geosciences, University of Oslo, Oslo, Norway, [3]Now at Department of Earth Sciences, University of Gothenburg, Göteborg, Sweden, [4]Department of Earth Sciences, Uppsala University, Uppsala, Sweden, [5]C.N.R.-Istituto sull'Inquinamento Atmosferico, Roma, Italy, [6]School of Environmental Sciences, University of East Anglia, Norwich, UK, [7]Department of Geography, University of Sheffield, Sheffield, UK, [8]LPC2E, UMR 7328, CNRS-Université d'Orléans, Orléans, France

Abstract The snowpack acts as a sink for atmospheric reactive nitrogen, but several postdeposition pathways have been reported to alter the concentration and isotopic composition of snow nitrate with implications for atmospheric boundary layer chemistry, ice core records, and terrestrial ecology following snow melt. Careful daily sampling of surface snow during winter (11–15 February 2010) and springtime (9 April to 5 May 2010) near Ny-Ålesund, Svalbard reveals a complex pattern of processes within the snowpack. Dry deposition was found to dominate over postdeposition losses, with a net nitrate deposition rate of (0.6 ± 0.2) μmol m^{-2} d^{-1} to homogeneous surface snow. At Ny-Ålesund, such surface dry deposition can either solely result from long-range atmospheric transport of oxidized nitrogen or include the redeposition of photolytic/bacterial emission originating from deeper snow layers. Our data further confirm that polar basin air masses bring ^{15}N-depleted nitrate to Svalbard, while high nitrate $\delta(^{18}O)$ values only occur in connection with ozone-depleted air, and show that these signatures are reflected in the deposited nitrate. Such ozone-depleted air is attributed to active halogen chemistry in the air masses advected to the site. However, here the Ny-Ålesund surface snow was shown to have an active role in the halogen dynamics for this region, as indicated by declining bromide concentrations and increasing nitrate $\delta(^{18}O)$, during high BrO (low-ozone) events. The data also indicate that the snowpack BrO-NO_x cycling continued in postevent periods, when ambient ozone and BrO levels recovered.

1. Introduction

1.1. Overview

Snowpack nitrate (NO_3^-) can influence the chemical composition of the lower atmospheric boundary layer through photochemical release of nitrogen oxides [e.g., *Honrath et al.*, 1999; *Domine and Shepson*, 2002; *Grannas et al.*, 2007; *Morin et al.*, 2009; *Thomas et al.*, 2012]. Even though snow is a highly reflective material, the shape and small size of snow grains favors a forward scattering of the light into the snowpack [*Domine et al.*, 2008], creating a photoactive zone in the surface region of the snow cover [e.g., *Qiu et al.*, 2002; *Simpson et al.*, 2002; *Galbavy et al.*, 2007]. Following polar sunrise, photolysis of surface snow NO_3^- and the concomitant emission of nitric oxide (NO) and nitrogen dioxide (NO_2) can alter the isotopic composition and concentration of NO_3^- in snow and ice [*Jarvis et al.*, 2008; *Frey et al.*, 2009; *Erbland et al.*, 2013]. Furthermore, the removal of NO_3^- through HNO_3 evaporation from snow can also contribute to NO_3^- isotopic and concentration changes [*Frey et al.*, 2009; *Erbland et al.*, 2013]. In addition to these postdeposition processes, dry deposition of pollutants and further accumulation of snow will influence the isotopic composition and budget of NO_3^-, where the snow accumulation buries older layers and prevents further photolytic reactions [*Jarvis et al.*, 2009; *Erbland et al.*, 2013]. Since several pathways have been described for the NO_x ($NO_x = NO + NO_2$) oxidation to nitric acid (HNO_3) in polar regions, e.g., involving ozone (O_3), hydroxyl (OH), and bromine monoxide (BrO) species [*Russell et al.*, 1985; *Evans et al.*, 2003; *Seinfeld and Pandis*, 2006; *Morin et al.*, 2007b], atmospheric boundary layer chemistry is of key importance for the isotopic NO_3^- signature found in snow.

Here we present a detailed investigation of the processes governing the concentration and isotopic composition of NO_3^- ($^{15}N/^{14}N$ and $^{18}O/^{16}O$) in the most photoactive zone (upper 5 cm) of the snowpack at

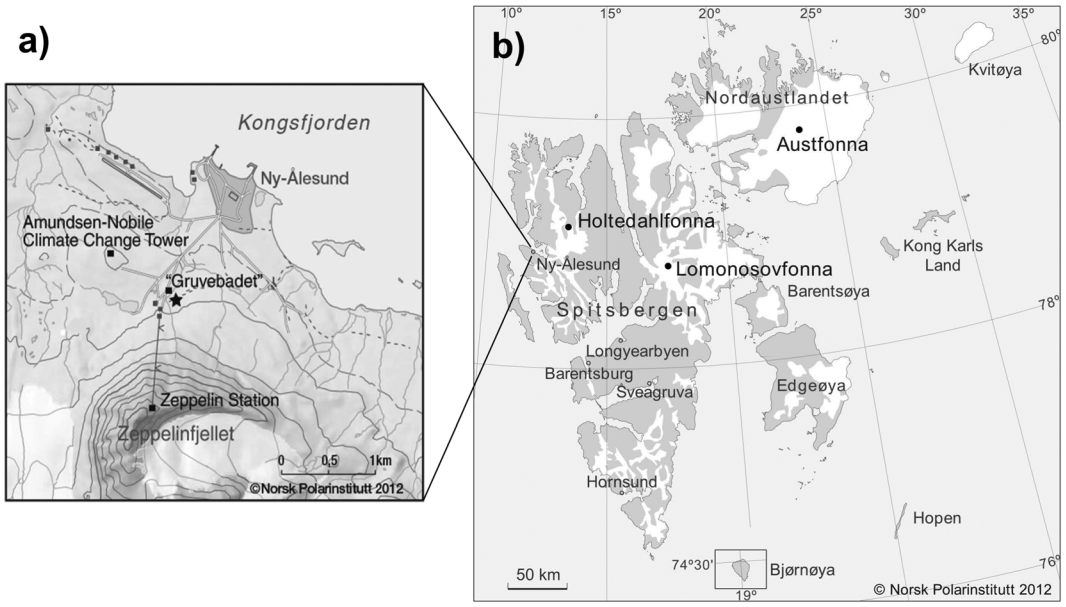

Figure 1. Maps of (a) the Ny-Ålesund region and (b) the Svalbard archipelago. Included in Figure 1a as a star is the surface snow sampling site and "Gruvebadet" (a newly established research site), the Amundsen-Nobile Climate Change Tower, and the Zeppelin Station. In Figure 1b the most commonly used ice core drilling sites (Holtedahlfonna, Lomonosovfonna, and Austfonna) are given along with the major settlements (Longyearbyen, Barentsburg, Svea, Ny-Ålesund, and Hornsund).

Ny-Ålesund, Svalbard (Figure 1). In order to highlight the effects of photolysis, the sampling period covered both the polar night and springtime during 2010. The data were analyzed in conjunction with atmospheric flux measurements of oxidized nitrogen; NO, NO_2, HNO_3, and particulate NO_3^- (p-NO_3^-), that were conducted directly above the snowpack, and O_3 concentrations monitored both at Gruvebadet and at the nearby Zeppelin Station (Figure 1). This study is used to infer the influence of BrO chemistry upon the snowpack nitrogen cycle for the first time in Svalbard.

1.2. Background

1.2.1. Long-Range Transport and Deposition of Oxidized Nitrogen

Through *long-range atmospheric transport* (Figure 2) oxidized nitrogen that is emitted at midlatitude regions can reach pristine Arctic environments [*Rahn et al.*, 1980; *Rahn*, 1981; *Dickerson*, 1985; *Stohl*, 2006; *Hirdman et al.*, 2010; *Kühnel et al.*, 2011; *Kühnel*, 2013], often in the form of molecules with longer atmospheric residence time such as peroxyacyl nitrates (PANs) or p-NO_3^- [*Beine et al.*, 1997; *Seinfeld and Pandis*, 2006]. However, occasional rapid long-range transport events also occur, as recently identified for Ny-Ålesund in the European high Arctic [e.g., *Hodson et al.*, 2010; *Kühnel*, 2013], which can transport pollutants with shorter lifetimes, such as NO_x, (or its oxidation product HNO_3) into the Arctic [*Zien et al.*, 2014]. The original isotopic composition of each NO_x source (e.g., forest fires or fossil fuel combustion, among other) depends on the oxidation process and origin of the nitrogen (N) and oxygen (O) [e.g. *Kendall et al.*, 2007]. In the Arctic spring, the long-range transported oxidized nitrogen pollutants, such as PANs, decompose and undergo local boundary layer *NO_x cycling*, involving O_3, BrO, or hydroperoxyl radicals (HO_2) and solar radiation (*hv*, Figure 2). This cycling is followed by a *NO_x removal*, where both a day time (through OH or HO_2) and a nighttime (through NO_3 and dinitrogen pentoxide (N_2O_5)) conversion of NO_2 to HNO_3 occurs (Figure 2) [*Russell et al.*, 1985; *Dentener and Crutzen*, 1993; *Hanson and Ravishankara*, 1995; *Hanson et al.*, 1996; *Evans et al.*, 2003; *Morin et al.*, 2007b; *Morin et al.*, 2008; *Thomas et al.*, 2011; *Thomas et al.*, 2012], where the N_2O_5 also can be directly deposited to the snow [e.g., *Huff et al.*, 2011]. For Arctic sites, HNO_3 production via the *BrO pathway*, involving $BrONO_2$ (Figure 2), is particularly important during episodes of BrO chemistry, which also causes low O_3 levels [e.g., *Evans et al.*, 2003; *Morin et al.*, 2007b]. Nitric acid and p-NO_3^- will then be removed from the atmosphere by snow, rain, or dry deposition [*Cadle*, 1991; *Bergin et al.*, 1995; *Kuhn*, 2001], and be deposited to the snow as NO_3^- [*Diehl et al.*, 1995; *Abbatt*, 1997]. The snowpack therefore acts as an important sink and reservoir for atmospheric reactive nitrogen, with a unique isotopic NO_3^- composition and

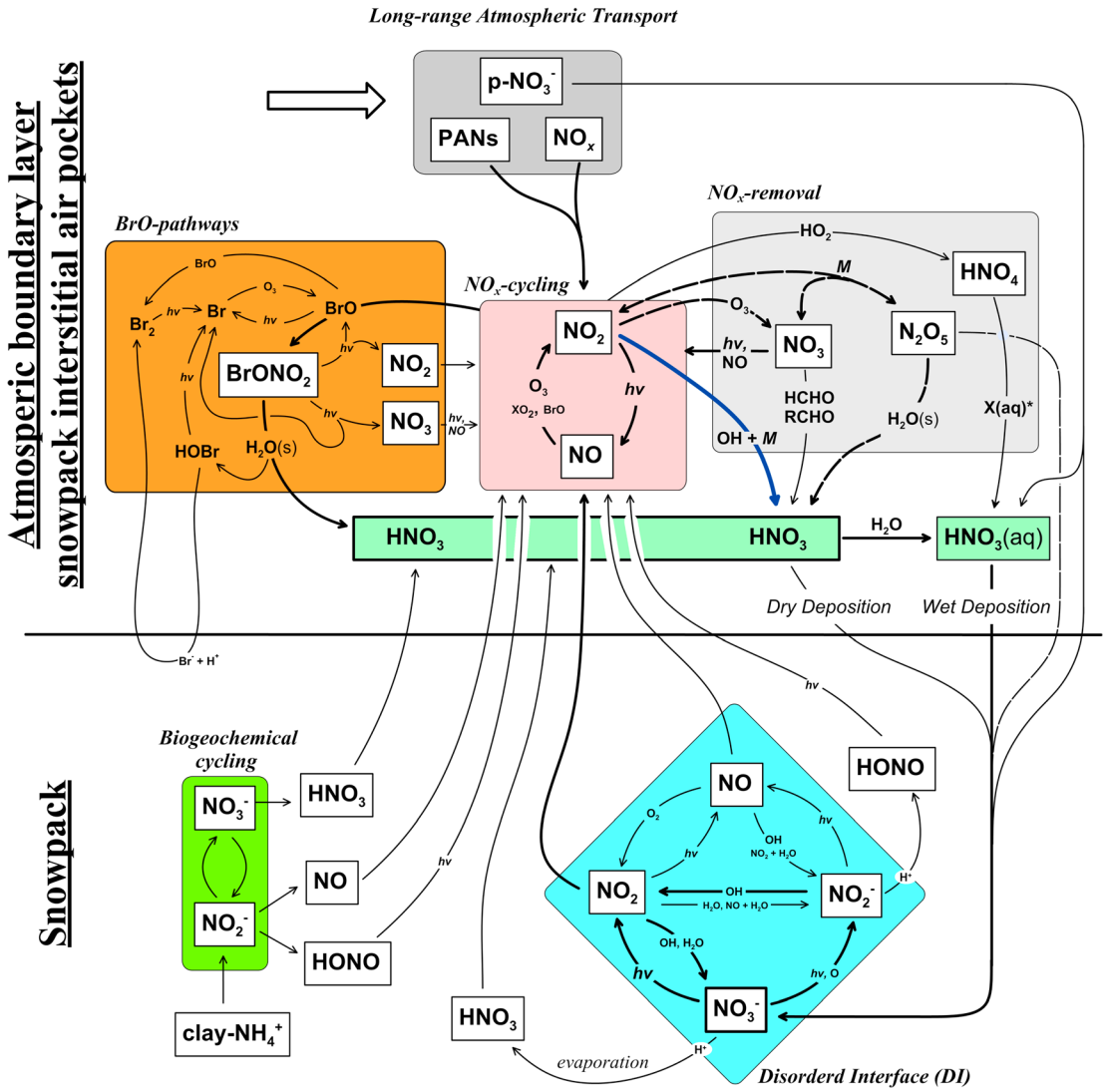

Figure 2. A schematic of the processes important for NO_3^- dynamics in Svalbard surface snow.

concentration for each snow layer. For the N-isotopic composition, the *initial* snow signature typically resembles the original source of NO_x, this since the fractionation during NO_x cycling and NO_x removal is considered to be low [*Freyer*, 1991]. For the O isotopes, the interaction and O exchange with O_3, BrO, and OH during the NO_x cycling and NO_x removal will strongly influence the initial snow O signature, typically masking any other processes or original source signatures [e.g., *Michalski et al*., 2003; *Jarvis et al*., 2009; *Morin et al*., 2009]. Thus the *initial* O signature provides insights into the oxidation processes that have occurred prior to deposition. These initial concentrations and isotopic imprints may, however, be altered by postdeposition processes as will be further outlined below (section 1.2.2).

In Svalbard, the NO_3^- deposition and thereby the snow concentration is governed by wet deposition, where a few sporadic "strong" events dominate the total annual deposition [*Kühnel et al*., 2011]. These strong deposition events are due to rapid transport of polluted European air masses [e.g., *Hodson et al*., 2010], which are occasionally channeled northward between a blocking anticyclone, situated over Scandinavia and Central Europe, and an incoming cyclone over the Atlantic [*Kühnel*, 2013]. The typical transport time for such events are about 2 to 5 days and where the air masses picks up in speed and humidity just prior to the arrival to Svalbard [*Kühnel*, 2013]. The estimated winter dry deposition of NO_3^- in this region is modest (approximately 14%) [*Björkman et al*., 2013], but nevertheless, of importance for the isotopic composition of NO_3^- in snow when studying short term daily variations [*Hastings et al*., 2004].

1.2.2. Snowpack NO_3^- Photolysis and Evaporation

Due to NO_x release from the photoactive zone of the snowpack, the deposited NO_3^- can play an important role in atmospheric boundary layer chemistry after the initial deposition [e.g., *Thomas et al*., 2012]. The snowpack is therefore an active player in atmospheric chemical processes and not just a NO_3^- sink [*Honrath et al*., 1999]. Snowpack NO_3^- photolysis, of relevance for the NO_3^- budget, is believed to occur at the very surface of snow crystals [*Boxe and Saiz-Lopez*, 2008], with reaction rates and quantum yields for photolytic processes similar to those in aqueous solutions [*Bartels-Rausch et al*., 2012]. This region of the ice crystal has previously been referred to as a quasi-liquid layer [*Kvlividz et al*., 1970], but has lately been redescribed as a disordered interface (DI) [*Bartels-Rausch et al*., 2012]. This new term emphasizes the disordered molecular structure that occurs at the surface of any crystal, created by the absence of molecular bonds toward its surface [*Bartels-Rausch et al*., 2012], instead of involving a liquid state analogy. The photolysis of NO_3^- within the DI and subsequent reactions (Figure 2) lead to the production of NO_2 and to a lesser extent NO (see *Jacobi and Hilker* [2007]; *Boxe and Saiz-Lopez* [2008] for an overview of reaction pathways). The produced NO_2 and NO can then diffuse out of the DI into firn air and thereafter into the atmospheric boundary layer [e.g. *Honrath et al*., 1999; *Jones et al*., 2000; *Beine et al*., 2003]. This photolytic initiated loss also alters the isotopic composition of snowpack NO_3^-, with an enrichment of ^{15}N in the residual NO_3^- due to photolytic fractionation [*Frey et al*., 2009; *Morin et al*., 2009; *Erbland et al*., 2013]. On the other hand the O composition of the remaining NO_3^- will be strongly influenced by the isotopic exchange between the photolytic products and OH-radical or H_2O within the DI [*McCabe et al*., 2005; *Frey et al*., 2009]. There is also evidence for nitrous acid (HONO) production from irradiated snow (Figure 2) [*Zhou et al*., 2001; *Beine et al*., 2002a], due to the interaction between nitrite (NO_2^-) and a hydrogen ion (H^+) [e.g., Dominé and Shepson, 2002]. However, several other pathways have also been described; i.e. involving humic acids [e.g., *Beine et al*., 2008; *Villena et al*., 2011] or heterogeneous reactions in the firn [e.g., *Jacobi and Hilker*, 2007], although the reaction steps in these pathways are not fully understood [*Grannas et al*., 2007; *Jacobi and Hilker*, 2007; *Beine et al*., 2008; *Boxe and Saiz-Lopez*, 2008; *Jacobi et al*., 2014] and therefore not included in Figure 2. Nitrate loss from the snow has also been found to be due to *evaporation* (Figure 2) of HNO_3, a process also favoring the loss of isotopically light NO_3^- [e.g., *Frey et al*., 2009]. A recent study by *Erbland et al*. [2013] confirms that evaporation is an active player in postdeposition processes in areas with low snow accumulation rates and high firn air ventilation, such as central Antarctic sites. However, the process has been shown to be quantitatively modest compared to the loss through photolysis for these Antarctic sites [*Erbland et al*., 2013]. Interestingly, laboratory studies of snow and ice have found no evidence for this evaporative pathway [*Chu and Anastasio*, 2003; *Sato et al*., 2008].

Snowpack NO_x emissions, according to the above postdeposition processes, have been estimated for Arctic, Antarctic, and midlatitude snow [*Dibb et al*., 1998; *Honrath et al*., 1999, 2000; *Jones et al*., 2000, 2001; *Beine et al*., 2002a]. However, these studies are not necessarily directly applicable to the snowpack in Ny-Ålesund, Svalbard (European high Arctic), where substantially lower snowpack NO_x, HNO_3, p-NO_3^-, and HONO emissions have been reported in comparison to the other investigated regions [*Beine et al*., 2003; *Amoroso et al*., 2006, 2010].

1.2.3. Local Biogeochemical Contribution to Snowpack NO_3^-

The DI reactions described above mostly involve NO_3^- of nonlocal origin, deposited following long-range atmospheric transport. However, a more locally produced source of oxidized nitrogen has been suggested through microbial activity [*Brooks et al*., 1997; *Ma et al*., 2007; *Miteva*, 2008; *Siciliano et al*., 2009; *Roberts et al*., 2010]. Svalbard snow is known to contain a diverse community of microorganisms [*Amato et al*., 2007; *Larose et al*., 2010], and the microbial assimilation of ammonium (NH_4^+) might result in the production of gas phase NO, HNO_3, and HONO, even during winter (Figure 2) [*Amoroso et al*., 2010]. Isotopic fractionation is expected through microbial assimilation of nitrogen compounds [e.g., *Kendall*, 1998], although during the nutrient-limited conditions in a snowpack such nitrogen isotopic fractionation might not necessarily be expressed in the produced reactive nitrogen emissions [*Amoroso et al*., 2010]. The resulting snowpack emission, under these conditions, would have an N isotopic composition related to the N source (in this case, organic or mineral bound NH_4^+) and an O isotopic composition influenced by the surrounding water [*Amoroso et al*., 2010].

1.2.4. Recycling of NO_x Snowpack Emissions

The gas phase products of postdeposition and biogeochemical processes are emitted into the firn air and onward to the lower atmospheric boundary layer, where further reactions may lead to a redeposition of

HNO_3 to the snow (Figure 2) [*Hastings et al*., 2004; *Morin et al*., 2007b; *Jarvis et al*., 2009]. During spring and summer conditions, these reactions can have a diurnal pattern governed by daytime emissions and nighttime deposition [*Hastings et al*., 2004]. The isotopic composition of this redeposited HNO_3 would then be influenced by the oxidation pathways undertaken, see Figure 2 [e.g., *Jarvis et al*., 2009]. Additionally, snow is a highly porous medium that undergoes a steady exchange of air with the surrounding atmosphere [*Sturm and Johnson*, 1991; *Albert and Hardy*, 1995; *Colbeck*, 1997; *Albert et al*., 2002; *Frey et al*., 2005]. This exchange allows the boundary layer processes in Figure 2 to occur also within the snowpack interstitial air pockets.

2. Methods

2.1. Field Sampling

The top 5 cm of the snowpack was sampled close to Gruvebadet, 1 km outside the *Ny-Ålesund International Arctic Research and Monitoring Facility* in Svalbard (78°55′N, 11°55′ E, Figure 1). Samples were collected between 11 and 15 February (*dark* campaign) and between 9 April and 5 May (*spring* campaign) during 2010. The sampling was undertaken at midday (11:00–13:00) during the dark campaign, and every morning (09:00 –10:00) during the spring campaign. All snow samples were collected by inserting a precleaned acrylic collars (height: 5 cm, inner diameter: 10.4 cm, and volume: 425 cm^{-3}) vertically into the snowpack, and using precleaned plastic shovels, clean overalls, face masks, and powder-free gloves. Triplicate samples were collected approximately 10 m apart, resulting in a total of 96 samples. To account for variations in surface snow density throughout the campaign, several collars were filled next to each other at each of the three triplicate sample locations, yielding a total sampled snow volume between 1.3 L and 3.8 L. The snow was transferred directly into clean black plastic zipper storage bags to prevent further photolysis, brought into the laboratory in Ny-Ålesund and melted at room temperature. Each melted snow sample was vacuum filtered (pore size 0.45 μm, according to *Hodson et al*. [2005]), bottled in 50 ml tubes, refrozen, and shipped for analysis of major ions and NO_3^- stable isotopes. To minimize contamination between samples, vacuum units and sample tubes were rinsed 3 times with sample water or, in the case of low sample volume, ultrapure water (>18 MΩ). Field blanks were collected along with the samples to check for contamination. Blank bags were opened and closed during sampling (without any snow addition), filled with 100 mL ultrapure water, and then treated and analyzed like the rest of the samples. Furthermore, during the spring campaign, an extra 50 ml sterile sampling tube was filled with the top 5 cm surface snow next to each sampling point for an opportunistic complementary major ion analysis performed on-site.

2.2. Laboratory Analysis

2.2.1. Major Ions

The samples were analyzed for NO_3^-, chloride (Cl^-), and sodium (Na^+) by ion chromatography at the Department of Geography, University of Sheffield, UK using two separate systems (Dionex DX 90 ion chromatographs, 4400 integrators, AS40 autosamplers) with Dionex columns AS14A and CS12A for anions and cations, respectively. Standards (range 100 to 2000 μg L^{-1}) were prepared every day from 1000 mg L^{-1} Merck CertiPUR stock standards. The analytical precision (1 standard deviation, 1σ) estimated from repeat analyses of multielement reference standards (Merck CertiPUR) were 1.4 and 1.6%, respectively, for the anions Cl^- and NO_3^-, and 0.06% for the cation Na^+. Based on repeat analyses of separate filter aliquots, the analytical precision including sample treatment was better than 5% for each ion. Detection limits (DL) defined as 3σ for the analytic blanks were 0.17, 0.21, and 0.34 μmol L^{-1} for Cl^-, NO_3^-, and Na^+, respectively.

The complementary springtime 50 ml snow samples and the diffusion line preparations (described below in section 2.3.2) were analyzed for NO_3^-, Cl^-, Na^+, NO_2^-, and bromide (Br^-) in Ny-Ålesund by the Institute of Atmospheric Pollution Research-National Research Council of Italy (IIA-CNR). Melted snow was analyzed without pretreatment by ion chromatography analytical technique (Dionex ICS 90 coupled with an AS50 autosampler and using Dionex AS14 and CS12 columns). A multipoint calibration was performed using six standards in the range 5 to 1000 μg L^{-1}, obtaining linear responses. Dilutions were carried out for more concentrated samples. Calibration solutions were prepared every second week from 1000 mg L^{-1} standard solutions (Merck). Control samples (1000 μg L^{-1} calibration solution) were analyzed every seven samples in order to recalibrate the ion chromatograph. The variation in the concentration of these control samples ranged within 0.5–1%. The analytical precision errors from repeated analyses of a calibration

solution (500 μg L^{-1}), were 1.13, 0.73, 0.35, 0.43, and 1.31%, respectively, for Cl^-, NO_2^-, Br^-, NO_3^-, and Na^+. Detection limits of 46. 5, 14.3, 4.9, 6.9, and 35.8 nmol L^{-1} were determined for Cl^-, NO_2^-, Br^-, NO_3^-, and Na^+, respectively.

2.2.2. NO_3^- Isotopic Composition

The ^{15}N and ^{18}O isotopic composition of NO_3^- were analyzed at the School of Environmental Sciences, University of East Anglia, Norwich, UK, using the bacterial denitrifier method [*Sigman et al*., 2001; *Coplen et al*., 2004; *Kaiser et al*., 2007] where the *Pseudomonas aureofaciens* strain was utilized. Values presented here are denoted as isotope deltas, $\delta(^{15}N)$ and $\delta(^{18}O)$ (IUPAC nomenclature: $\delta(^{15}N, ^{14}N, NO_3^-)$ and $\delta(^{18}O, ^{16}O, NO_3^-)$, respectively), and expressed with respect to an international standard in ‰ (10^{-3}, per mil) (equation (1)).

$$\delta_{\text{sample}} = \frac{R_{\text{sample}} - R_{\text{ref}}}{R_{\text{ref}}} \tag{1}$$

Here R represents the $^{15}N/^{14}N$ or $^{18}O/^{16}O$ ratio in the sample ($_{\text{sample}}$) and reference ($_{\text{ref}}$) respectively, where atmospheric nitrogen (Air-N_2) was used as nitrogen reference and Vienna Standard Mean Ocean Water (VSMOW) was used as oxygen reference. Positive delta values indicate an enrichment of the heavier isotope (or a depletion of the lighter isotope) compared to the standard. To calibrate the isotope delta values, the international nitrate reference material IAEA-NO-3 was used, assuming it has $\delta(^{15}N) = 4.7‰$ versus Air-N_2 and $\delta(^{18}O) = 25.61‰$ versus VSMOW [*Böhlke et al*., 2003]. The $\delta(^{15}N)$ values reported here have not been corrected for any nonmass-dependent ^{17}O contribution to the *m/z* 45 ion current during mass spectrometric analysis. However, $\delta((17)O)$ and $\delta(^{18}O)$ are usually well correlated and the true $\delta(^{15}N)$ was estimated to be 1–2‰ lower than the reported values. The bacterial denitrifier method requires a minimum of 20 nmol NO_3^- (optimum being 50 nmol) in at most 10 mL of solution. Consequently, only samples above this limit were analyzed ($n = 87$).

2.3. Air-Snow Fluxes

2.3.1. Surface Snow Net Change

By following the concentration change in surface snow over time, it is possible to evaluate the overall net change due to processes occurring after wet deposition. This method has previously been used to evaluate NO_3^- dry deposition to snow [*Cadle et al*., 1985; *Johansson and Granat*, 1986; *Cadle*, 1991; *Cress et al*., 1995]. The net change (F_{net}) can be calculated as [*Björkman et al*., 2013]:

$$F_{\text{net}} = -\frac{c_0 V_t - c_t V_t}{At} \tag{2}$$

where c is the molar NO_3^- concentration in snow, V the melted volume of the sample, A the surface area of the snow sample (in this study equal to the cross-section area of the sampling collar), and where t is the exposure time between the initial sample (index: 0) and the final sample (index: t). In *Björkman et al*. [2013], the dry deposition was calculated as an atmospheric loss, giving negative numbers, whereas here the surface gain is of interest; hence, a negative sign is used in equation (2) to account for this. Furthermore, equation (2) will be valid as a pure dry deposition estimate only if no other NO_3^- postdeposition processes take place and snow water sublimation is negligible. In all other cases, equation (2) will describe the net effect of the various processes. In terms of the isotopic composition, equation (2) can be written as:

$$F_{\text{net}}\,(1 + \delta_{\text{net}}) = -k\,[c_0(1 + \delta_0) - c_t(1 + \delta_t)] \tag{3}$$

where k is the deposition velocity given as: $k = V_t / (At)$, δ_{net} is the isotopic composition of the net change, whereas δ_0 and δ_t are the initial and final isotopic composition of NO_3^-. Equation (3) can be expressed as

$$0 = c_t(\delta_t - \delta_{\text{net}}) - c_0(\delta_0 - \delta_{\text{net}}) \tag{4}$$

which then can be rearranged to give

$$\delta_{\text{net}} = \frac{c_t\delta_t - c_0\delta_0}{c_t - c_0} \tag{5}$$

equation (5) then gives the change in the isotopic signature (δ_{net}) and is equal to the isotopic composition of the dry deposited NO_3^- if other postdeposition processes are negligible.

2.3.2. NO_x, HNO_3^-, and p-NO_3^- Flux Measurements

In addition to the snow sampling, atmospheric flux measurements of NO, NO_2, HNO_3, and p-NO_3^- to and from the snowpack were conducted by IIA-CNR outside Gruvebadet (200 m from the snow sampling site)

during the period 9 to 27 April in 2010. The NO and NO_2 concentrations were measured on a 6 min basis, using a modified commercial two-channel high-sensitivity chemiluminescence detector (Sonoma Technologies, USA) [*Beine et al*., 2002b; *Amoroso et al*., 2010]. The two channels sampled air from dual inlets at 0.3 m and 1.5 m above the surface snow, respectively. Nitric oxide detection was based on the chemiluminescence signal produced by the reaction between NO and O_3, which was photolytically generated in a 150 mL min^{-1} flow rate of O_2 by a corona discharge O_3 generator. Nitrogen dioxide was detected as NO following photolysis between 350 and 420 nm by light-emitting diodes. The instrument was calibrated daily with 5.0 μmol mol^{-1} of gaseous NO (NIST traceable NO standard, Scott-Marrin, in N_2) at a flow rate of 2.0 mL min^{-1} into the sampling flow (about 1200 mL min^{-1}), corresponding to a NO addition of 8.3 nmol mol^{-1}. The NO detection limit was determined as 3σ of the observed scatter in the instrument signal and corresponded to 2.5 pmol mol^{-1} for 1 h averages.

Measurements of HNO_3 and p-NO_3^- concentrations were made by two independent diffusion lines [*Beine et al*., 2001; *Perrino et al*., 2001; *Ianniello et al*., 2002, 2007] with inlets also at 0.3 and 1.5 m above the snow surface. The HNO_3 and p-NO_3^- concentration was measured on a 12 h basis from 10 to 16 April, while a time resolution of 24 h was used from 17 to 27 April. The diffusion lines used in this study included a denuder train consisting of two sodium fluoride (1% NaF in 9:1 ethanol/water solution) coated denuders for HNO_3 sampling. The atmospheric HNO_3 concentrations were calculated by subtracting the analyte mass (expressed as NO_3^-) in the second NaF coated denuder from the analyte mass in the first NaF coated denuder [*Febo et al*., 1989]. The denuder train was followed by a cyclone (2.5 μm aerodynamic diameter cutoff point) and a filter pack set in series, for the collection of particulate matter in the coarse and fine fractions, respectively. The filter pack included a Teflon filter (Whatman Teflon, 47 mm, 1 μm pore size), a nylon filter (Nylosorb Gelman, 47 mm, 1 μm pore size), a Na_2CO_3 glycerol-impregnated paper filter (Whatman 41) and a H_3PO_3 coated paper filter. The last three filters were used to collect chemical species evaporated from the Teflon filter [*Ianniello et al*., 2002, 2011; *Spataro et al*., 2013]. The sampling flow rate was 15 L min^{-1}, and typical sampling volumes of 11.9 m^3 and 23.5 m^3 were obtained for 12 h and 24 h sampling periods, respectively. After sampling, the denuders, cyclone, and filters were extracted and these samples were analyzed within 24 h by using the IIA-CNR Ion Chromatography system described in section 2.2.1. Under these conditions, the collection efficiency for both HNO_3 and p-NO_3^- was >99%. The DL of HNO_3 and p-NO_3^- (calculated as 3σ of field blanks) were 2.95 ng m^{-3} and 1.42 ng m^{-3}, respectively, on a 24 h measurement period, while the precision errors of these measurements were 2.54% at 20 ng m^{-3} and 0.73% at 79 ng m^{-3}, respectively. Here we focus only on HNO_3 and p-NO_3^- data, although the diffusion line sampling system did allow us to also collect other gaseous and particulate compounds, which will be discussed elsewhere.

The fluxes of NO, NO_2, HNO_3, and p-NO_3^- (hereafter F_{NO}, F_{NO2}, F_{HNO3}, and $F_{p\text{-}NO3}$, respectively) were determined combining the two height gradient sampling with atmospheric turbulence measurements. The difference between the measured concentrations at the two sampling heights is in this work referred to a concentration difference (Δ = lower height − upper). Hence, a positive difference implies emission of the measured species from the snow surface.

Using the measured concentration differences and the atmospheric eddy diffusivities (K) for the same period, the atmospheric fluxes for NO, NO_2, HNO_3, and coarse and fine particulate NO_3^- were derived (Flux = $\Delta \times K$) as detailed elsewhere [*Sozzi et al*., 1998; *Ianniello et al*., 2002; *Beine et al*., 2003, and references therein]. Diffusivities were obtained from atmospheric turbulence measurements made at a frequency of 10 Hz by using an sonic anemometer (Metek, USA-T1), which was placed at 1.5 m above the snowpack, assuming neutral boundary layer conditions.

For the purpose of this study these fluxes have been averaged to daily emissions, depositions, and net fluxes (from 09:00 onward) for comparison with the surface snow data.

2.3.3. Dry Deposition Estimates

If the atmospheric concentration (c_{atm}) of HNO_3 and p-NO_3^- are measured, the expected dry deposition flux ($F_{dry\text{-}dep}$) can be modeled as long as the deposition velocities (v_d) are known [e.g., *Seinfeld and Pandis*, 2006]:

$$F_{dry-dep} = v_d c_{atm} \quad (6)$$

In a recent study covering the same spring campaign, the dry deposition of HNO_3 and p-NO_3^- was both modeled and measured for Ny-Ålesund [*Björkman et al*., 2013]. Median deposition velocities were estimated

to be 0.63 cm s^{-1} for HNO_3 and 0.0025 or 0.16 cm s^{-1} for p-NO_3^-, particle size 0.7 and 7 μm in diameter, respectively [*Björkman et al*., 2013]. The combined gaseous and particulate dry deposition, F_{model}(LND) (referring to the modeled HNO_3 and p-NO_3^- dry deposition rates obtained using a lognormal distribution (LND) for NO_3^- aerosols sizes in *Björkman et al*. [2013]), will be used here for comparison with the surface snow and flux measurements, and for further modeling purposes. *Björkman et al*. [2013] also measured the actual NO_3^- dry deposition (F_{tray}) to snow using a "bucket" approach [e.g., *Cress et al*., 1995] and found an average deposition of (0.04 ± 0.02) mg m^{-2} d^{-1} (equal to (0.7 ± 0.3) μmol m^{-2} d^{-1}) which will also be used for further modeling purposes. An overview of NO_3^- dry deposition in the Arctic, and a full description of these dry deposition estimates are given by *Björkman et al*. [2013].

2.3.4. Additional Observations

Meteorological data from Ny-Ålesund, in particular precipitation data, were provided by the Norwegian Meteorological Institute (DNMI) and are available at http://www.eklima.no. The atmospheric concentration of O_3 (c_{O3}) is continuously measured by the Norwegian Institute for Air Research (NILU) at the nearby Zeppelin atmospheric research station (474 m above sea level, Figure 1), available at http://ebas.nilu.no. During the spring campaign 2010, O_3 concentrations were also recorded by IIA-CNR at Gruvebadet until 27 April. NILU also provides an online base atmospheric transport model, FLEXTRA (http://www.nilu.no/projects/ccc/trajectories/). Using FLEXTRA air mass back trajectories arriving to Ny-Ålesund were established for all sampling days at 00:00 and 12:00, with trajectories spanning 7 days back in time.

Additionally, sonic anemometer (Gill R3) and fast hygrometer (Campbell Scientific KH2O krypton) data from the Amundsen-Nobile Climate Change Tower (Figure 1) were provided by The Institute for Atmospheric Science and Climate-National Research Council of Italy (ISAC-CNR, M. Mazzola, and A. Viola, personal communication, 2013). The 10 min average data sampled at 7.5 m above ground were used to evaluate water vapor flux as an indication of sublimation rates.

2.4. Models

2.4.1. Photolytic Model

NO_x production due to photolysis of NO_3^- has previously been modeled for Ny-Ålesund snow, using the solar zenith angle (θ_{SZA}) and the surface snow NO_3^- concentrations, with results comparable to NO_x emission measurements [*France et al*., 2010, 2011b]. This model assumes that the photolysis of NO_3^- only follows the reaction $NO_3^- + h\nu \rightarrow NO_2 + O^-$ and is, according to the reactions in Figure 2, a simplification of the DI dynamics but has the potential to provide useful insights into the NO_3^- loss through photolysis. For the purpose of this study, a photolytic rate function considering only the surface snow layer during clear-sky conditions [*France et al*., 2010] will be used for comparison to the sampled top 5 cm of the snowpack. However, a depth-integrated model would be more appropriate if bulk snowpack samples were under consideration (see *France et al*. [2010, 2011a, 2011b] for further details). Here only surface snow was sampled, in order to avoid a potential disturbance of the postdeposition processes under investigation.

A polynomial function (equation (7)) was fitted to the photolysis rates (J_{NO3-}, in s^{-1}) given in *France et al*. [2010] as a function of θ_{SZA} (in degrees), with $R^2 = 0.9994$ (Figure S1 in the supporting information):

$$J_{NO_3^-} = 1.18e^{-14}\theta_{SZA}{}^4 - 1.09e^{-12}\theta_{SZA}{}^3 - 3.51e^{-11}\theta_{SZA}{}^2 - 8.80e^{-10}\theta_{SZA} + 3.86e^{-7} \quad (7)$$

where θ_{SZA} was extracted for Ny-Ålesund (http://www.esrl.noaa.gov/gmd/grad/neubrew/) with 1 h resolution. Furthermore, to not induce any error from equation (7) when the Sun is close to or below the horizon, J_{NO3-} was set to zero for $\theta_{SZA} > 89.77°$.

The upper limit for the surface snow NO_2 emission ($F_{J\ NO3-}$) can then be calculated as

$$F_{J_{NO_3^-}} = J_{NO_3^-} c_0 z_{SWE} \quad (8)$$

where c_0 is the concentration of NO_3^- (in mol m^{-3}) and z_{SWE} is the snow water equivalence of the surface snow (in meters). For lower NO_3^- concentrations, or unusually high NO_2 emissions, the surface snow NO_3^- concentration might change over the course of the day. To minimize this potential source of error, the time resolution of the photolysis calculations was set to 1 h in accordance with the θ_{SZA} data. The $F_{J\ NO3-}$ emission given by equation (8) provides the flux in μmol m^{-2} d^{-1} units.

2.4.2. Box Models

A box model, describing the main sources and sinks of NO_3^- in the snow, was applied to predict changes in concentration (c_{NO3}), $\delta(^{15}N)$, and $\delta(^{18}O)$ of NO_3^-. In this box model all outgoing fluxes were assumed to be due to photolysis of NO_3^-, and all incoming fluxes were assumed to be due to NO_3^- dry deposition. Hence, this is a simplification of the actual processes, which might, for example, also include evaporation of HNO_3 (see Figure 2). However, as an initial assumption (and further justified below) photochemistry was assumed to be the major loss process for this surface snow study.

In the model, the change in c_{NO3} over time when the Sun is below the horizon was expressed as equation (9), while equation (10) gives the change when both dry deposition and photolysis are present

$$\frac{dc}{dt} = \frac{v_d c_{atm} A}{V_t} \tag{9}$$

$$\frac{dc}{dt} = \frac{v_d c_{atm} A}{V_t} - Jc \tag{10}$$

Here $v_d c_{atm}$ equals the dry deposition rates according to equation (8) and was attributed to the F_{model}(LND) or F_{tray} in *Björkman et al*. [2013], while the product of photolytic rate (J) and snowpack concentration (c) constitutes the loss process. Note, in equation (10) and the following equations the photolytic rate of NO_3^- (J_{NO3^-} in equation (7)) has been substituted with J to keep the equations simple. Equations (9) and (10) can be integrated to give the new concentration (c_t):

$$c_t = \frac{v_d c_{atm} A t}{V_t} + c_0 \tag{11}$$

$$c_t = \left(\frac{v_d c_{atm} A}{V_t J}\right) * \left(1 - e^{-Jt}\right) + c_0 e^{-Jt} \tag{12}$$

where equations (11) and (12) represent periods when the Sun is below or above the horizon, respectively. The isotopic composition of NO_3^- remaining in the snow (δ_t) can then be expressed as

$$\delta_t = \left(\frac{c'_t}{c_t} - 1\right) / R_{ref} \tag{13}$$

Similar to equations (11) and (12), c'_t are given by

$$c'_t = \frac{v_d c'_{atm} A t}{V_t} + c'_0 \tag{14}$$

$$c'_t = \left(\frac{v_d c'_{atm} A}{V_t J'}\right) * \left(1 - e^{-J't}\right) + c'_0 e^{-J't} \tag{15}$$

where $c'_0 = c_0 R_{ref}(1+\delta_0)$, $c'_{atm} = c_{atm} R_{ref}(1+\delta_{atm})$, and $J' = J(1+\varepsilon)$, and where δ_0 and δ_{atm} are the initial and atmospheric N or O isotopic composition, respectively, while ε is the photolytic fractionation for $^{15}N/^{14}N$ ($^{15}\varepsilon$) and $^{18}O/^{16}O$ ($^{18}\varepsilon$). Primed quantities refer to the less abundant isotopic species (^{15}N or ^{18}O). The error due to the assumption that the concentration of the major isotope is equal to the total nitrate concentration, is negligible (<0.01‰).

In order to evaluate the daily $\delta(^{15}N)$, $\delta(^{18}O)$, and c_{NO3} changes induced from the NO_x, HNO_3^-, and p-NO_3^- flux measurements (section 2.3.2), the daily averaged emissions (F_{emi}) and deposition (F_{dep}) were evaluated in a similar way:

$$c_t = \frac{F_{(dep)} A t}{V_t} - \frac{F_{(emi)} A t}{V_t} + c_0 \tag{16}$$

$$c'_t = \frac{F'_{(dep)} A t}{V_t} - \frac{F'_{(emi)} A t}{V_t} + c'_0 \tag{17}$$

where $F'_{(dep)} = F_{(dep)} R_{ref}(1+\delta_{atm})$, $F'_{(emi)} = F_{(emi)} R_{ref}(1+\delta_{photo})$, and δ_{photo} is the isotopic composition of the instantaneous photolytic product: $\delta_{photo} = \delta_0(1+\varepsilon) + \varepsilon$.

Previous studies have suggested a range of $^{15}\varepsilon$, from −48‰ [*Frey et al*., 2009] to −12‰ [*Blunier et al*., 2005], and $^{18}\varepsilon$ from −34‰ [*Frey et al*., 2009] to between 2 and 7‰ [*McCabe et al*., 2005] for the photolytic

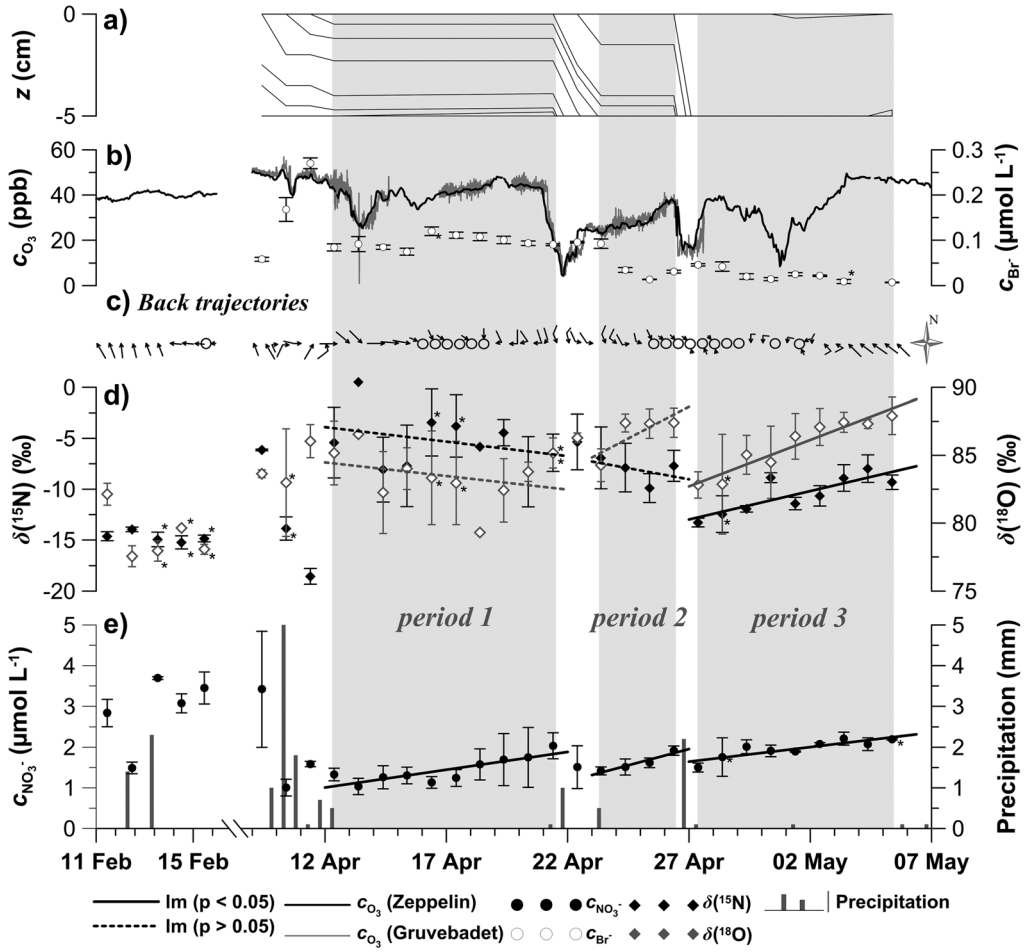

Figure 3. Nitrate concentrations (c_{NO3}) and isotopic signatures ($\delta(^{15}N)$ and $\delta(^{18}O)$) of the daily surface snow samples in 2010, including (a) a schematic sketch of the visible layering found in the sampled surface snow; (b) the atmospheric O_3 concentration (c_{O3}) measured at the Zeppelin Station and at Gruvebadet, along with surface snow Br^- concentrations (c_{Br}); (c) a schematic sketch of 7 days back trajectories obtained from the FLEXTRA model, where arrows indicate flow paths and circles indicate stagnant air; (d) the measured $\delta(^{15}N)$ and $\delta(^{18}O)$ in the surface snow; and (e) the measured c_{NO3} in the surface snow together with the registered precipitation in Ny-Ålesund. Furthermore, error bars indicates standard error ($\sigma_{\bar{x}}$), asterisks indicate samples where $\sigma_{\bar{x}}$ is calculated from only two data points, and symbols without error bars indicates one replicate. Solid lines represent significant linear regression models (lm, p value < 0.05), while broken lines equal non-significant trends (p value > 0.05).

fractionation in question. However, secondary reactions (e.g., $NO_2 + OH^- \rightarrow NO_3^-$) following photolysis will generate an exchange of O (see DI reactions in Figure 2) [*Jacobi and Hilker*, 2007] suggesting that any measured estimation of $^{18}\varepsilon$ will represent the combined effect of both the photolytic fractionation and secondary reactions [*McCabe et al*., 2005; *Erbland et al*., 2013]. For the purpose of this study, $^{15}\varepsilon$ and $^{18}\varepsilon$ were set to −48 and 2‰, respectively [*McCabe et al*., 2005; *Frey et al*., 2009]. Furthermore, a sensitivity test covering a range from 0 to −70‰ for $^{15}\varepsilon$ and 10 to −50‰ for $^{18}\varepsilon$ was also performed to evaluate the actual influence of different photolytic fractionations on the results.

Furthermore, three δ_{atm} deposition scenarios for each isotope composition, $\delta(^{15}N)$ and $\delta(^{18}O)$, were evaluated with the aim of establishing the most likely input source, so called "end-member," signatures for any dry deposition. For $\delta_{atm}(^{15}N)$ these scenarios were set to resemble the following: (i) the local biogeochemical signal (+5‰), (ii) the ambient atmospheric signal (−13‰) described for Ny-Ålesund by *Amoroso et al*. [2010], and (iii) the influence of Polar basin air (−20‰) suggested by *Morin et al*. [2009]. For $\delta_{atm}(^{18}O)$ the scenarios were set to resemble the following: (i) the low $\delta(^{18}O)$ signal found in HNO_3 at Summit, Greenland (+40‰), due to the interaction with OH during NO_x cycling and removal (see Figure 2) [*Jarvis et al*., 2009], (ii) the

Table 1. Fitted Linear Regression Models ($y = kx + m$) for the Three Periods (Figure 4)[a]

Model	Period	k	m	n	R^2	p value	Unit
c_{NO3}	1	0.1	−7.8	30	0.17	< 0.03	μmol L^{-1}
	2	0.2	−18.1	12	0.50	0.01	μmol L^{-1}
	3	0.1	−6.5	26	0.34	< 0.01	μmol L^{-1}
c_{Br}	1	1.5	−61.3	29	0.06	0.18	nmol L^{-1}
	2	−20.6	2100.4	12	0.56	< 0.01	nmol L^{-1}
	3	−4.5	566.2	23	0.56	≪ 0.01	nmol L^{-1}
c_{Cl}	1	2.4	−206.6	29	0.09	0.11	μmol L^{-1}
	2	3.4	−348.0	12	0.04	0.56	μmol L^{-1}
	3	3. 1	−339.7	26	0.45	< 0.01	μmol L^{-1}
c_{Na}	1	1.0	−70.8	30	0.02	0.42	μmol L^{-1}
	2	2.7	−279.4	12	0.06	0.43	μmol L^{-1}
	3	3.2	−354.8	27	0.40	< 0.01	μmol L^{-1}
$\delta(^{15}N)$	1	−0.1	8.8	23	0.01	0.67	‰
	2	−0.4	41.6	12	0.02	0.65	‰
	3	0.6	−85.1	26	0.49	< 0.01	‰
$\delta(^{18}O)$	1	−0.1	90.2	23	0.00	0.78	‰
	2	0.9	−20.7	12	0.28	0.08	‰
	3	0.7	−0.4	26	0.37	< 0.01	‰
z_{SWE}	1	0.1	−8.2	30	0.50	≪ 0.01	cm
	2	0.03	−2.0	12	0.02	0.63	cm
	3	0.2	−21.1	26	0.88	≪ 0.01	cm
V	1	4.0	−346.8	30	0.50	≪ 0.01	mL
	2	−0.7	−157.3	12	0.01	0.80	mL
	3	7. 8	−896.6	26	0.88	≪ 0.01	mL

[a]Regression models where analyzed for the NO_3^- concentration (c_{NO3}), Br^- concentration (c_{Br}), Cl^- concentration (c_{Cl}), Na^+ concentration (c_{Na}), the NO_3^- isotopic composition ($\delta(^{15}N)$ and $\delta(^{18}O)$), the surface snow water equivalence (z_{SWE}), and the sample volume (V). Also given are the numbers of measurements (n) used for each regression, the multiple R^2 value for the models, and the significance (p value) of the slope k.

midlatitude HNO_3 signal (+75‰) found in air arriving at Svalbard [*Morin et al.*, 2009], and (iii) the uniquely high $\delta(^{18}O)$ found for HNO_3 in the polar basin atmosphere during spring due to the influence of the BrO pathway (up to +100‰, *Morin et al.*, 2009).

3. Results

3.1. NO_3^- Concentrations

The surface snow NO_3^- concentrations (c_{NO3}) during the dark ($n = 14$) and the spring ($n = 79$) campaign averaged (2.9 ± 0.2) μmol L^{-1} and (1.7 ± 0.1) μmol L^{-1}, respectively (where the uncertainty denotes the standard error, $\sigma_{\bar{x}}$), with a total concentration range from 0.6 to 6.3 μmol L^{-1} (Figure 3e). The variations among the three replicates, sampled approximately 10 m apart, were moderate (average $\sigma_{\bar{x}} = 0.3$ μmol L^{-1}) with some exceptions (maximum $\sigma_{\bar{x}} = 1.4$ μmol L^{-1} on 9 April), as viewed by the occasionally increased $\sigma_{\bar{x}}$ in Figure 3e. The c_{NO3} variation found is larger than the errors expected from IC analysis itself and therefore shows that local variation and the layering of the surface snow have a large influence. During both the dark and the spring campaign, several precipitation events occurred (Figure 3e) which introduced new snow layers with event-specific NO_3^- concentration and isotopic signature. These events interrupted any trends that postdeposition processes would have introduced to the surface snow chemistry, and the spring data were therefore separated into three distinct, precipitation-free periods: 12–21, 23–26, and 27 April to 5 May (Figure 3). Periods 1 and 2 were characterized by multiple surface snow layers, whereas period 3 followed a large (>5 cm) precipitation event resulting in a relatively uniform snow surface (Figure 3a). Period 3 was therefore considered the most reliable period for identification of c_{NO3} and isotope composition trends.

For the spring campaign, linear regression models fitted to all three periods showed significant increases in the surface snow c_{NO3} (Figure 3e and Table 1), indicative of net deposition or snow water sublimation (see section 3.4). No such changes were found during the short dark sampling campaign due to interrupting precipitation events. In general, all three spring periods indicated a day to day c_{NO3} variation. To avoid any bias caused by such

Table 2. Calculated Initial ($_0$) and Final ($_t$) Values From the Regression Model in Table 1

Model	Period	0	t	Unit
c_{NO3}	1	1.1 ± 0.2	1.8 ± 0.2	μmol L^{-1}
	2	1.4 ± 0.1	1.9 ± 0.1	μmol L^{-1}
	3	1.7 ± 0.1	2.3 ± 0.1	μmol L^{-1}
$\delta(^{15}N)$	1	−5.3 ± 1.8	−6.5 ± 1.7	‰
	2	−7.4 ± 1.7	−8.7 ± 1.7	‰
	3	−12.9 ± 0.6	−8.0 ± 0.6	‰
$\delta(^{18}O)$	1	84.0 ± 1.2	83.4 ± 1.2	‰
	2	85.2 ± 0.9	88.0 ± 0.9	‰
	3	83.0 ± 0.9	88.7 ± 0.9	‰
z_{SWE}	1	1.3 ± 0.1	2.2 ± 0.1	cm
	2	1.7 ± 0.1	1.8 ± 0.1	cm
	3	0.4 ± 0.1	1.8 ± 0.1	cm
V	1	57.2 ± 4.0	92.9 ± 4.0	mL
	2	73.4 ± 5.2	71.2 ± 5.2	mL
	3	15.6 ± 2.9	78.0 ± 2.9	mL

variation, the fitted linear regression models were used to calculate initial (index: 0) and final (index: t) values of c_{NO3} (and other relevant parameters) for each period and will be used for modeling purposes (Tables 1 and 2).

3.2. NO_3^- Isotopic Composition

The $\delta(^{15}N)$ of NO_3^- ranged between −15.9 and −13.7‰ during the dark sampling ($n = 12$) and between −19.9 and 0.7‰ during the spring campaign ($n = 71$), averaging (−14.7 ± 0.2) ‰ and (−8.7 ± 0.5) ‰, respectively (Figure 3d). The $\delta(^{18}O)$ ranged between 76.6 and 83.7‰ during the dark sampling and 76.5 to 90.6‰ during the spring campaign, averaging (79.2 ± 0.6) ‰ and (85.1 ± 0.4) ‰, respectively (Figure 3d). In summary, the spring snow has significantly elevated values of $\delta(^{15}N)$ and $\delta(^{18}O)$ compared to the dark sampling (p value < 0.01), although both periods showed considerable variability.

Linear regression models revealed significant increases of $\delta(^{15}N)$ and $\delta(^{18}O)$ during period 3 (Table 1), and to a lesser extent (p value = 0.08) for $\delta(^{18}O)$ during period 2 (Figure 3d and Table 1). The remaining linear regression models fitted for $\delta(^{15}N)$ and $\delta(^{18}O)$ during period 1 and 2 were not significant (Figure 3d and Table 1). In a similar manner to c_{NO3}, the initial and final $\delta(^{15}N)$ and $\delta(^{18}O)$ values were calculated for each period using the linear regression models (Tables 1 and 2) to minimize the effects of daily variability upon further calculations.

3.3. Snow Br^- and Atmospheric O_3 Concentrations

In contrast to c_{NO3}, surface snow concentration of Br^- (c_{Br}) showed an overall linear decline, particularly during periods 2 and 3 (Figure 3b and Table 1). This decline was in clear contrast to the observed sea salt deposition, as shown by the linear regression models fitted to the surface snow Na^+ and Cl^- concentrations (c_{Na} and c_{Cl}, respectively, in Table 1). The most likely explanation for this c_{Br} depletion involves BrO chemistry (discussed in section 4.4), which is typically connected to changes in atmospheric O_3 concentration (c_{O3}). The ambient c_{O3} showed evidence for several ozone depletion events (ODEs) during the spring campaign. These ODEs mainly occurred during periods 2 and 3 and were commonly associated with air mass back trajectories arriving from the polar basin (Figures 3b and 3c).

3.4. Sublimation Rates

The measurement of water vapor fluxes during the campaign was challenging due to riming or fog on the optical windows of the fast hygrometer, meaning that calibration was not always possible, which reduced the number of valid measurements. The removal of outliers from the sonic anemometer data further reduced the data to a final count of 282 measurements throughout the precipitation-free subperiods. Nevertheless, the data confirm a low sublimation rate: the water vapor fluxes indicated an average sublimation rate of (−0.042 ± 0.002) mm d^{-1} ($n = 282$), where the total water vapor flux spanned between −0.007 and 0.008 mm h^{-1} (negative flux indicates surface loss). This sublimation rate has a very small impact on surface snow NO_3^- concentration as discussed below.

3.5. Air-Snow Fluxes

3.5.1. Surface Snow Net Change

The increasing trends in surface snow c_{NO3} indicate a net deposition of NO_3^- since snow water sublimation was found to be low. Hence, this indicated that dry deposition rates overcome photolytic and evaporative losses. Using the calculated initial and final values of c_{NO3} and V for each period (Table 2), all three periods

Table 3. Calculated net Change of NO_3^- (F_{net}) and Isotopic Signatures ($\delta(^{15}N)$ and $\delta(^{18}O)$)

Period	F_{net}[a] ($\mu mol\ m^{-2}\ d^{-1}$)	$\delta(^{15}N)$[b] (‰)	$\delta(^{18}O)$[b] (‰)
1	0.9 ± 0.4	−8.2 ± 13.6	82.7 ± 87.9
2	1.4 ± 0.6	−12.2 ± 18.8	95.4 ± 110.6
3	0.6 ± 0.2	7.0 ± 5.6	105.9 ± 72.3

[a]Calculated from equation (2).
[b]Calculated from equation (5).

were confirmed to have a significant increase due to net deposition according to equation (2) (Table 3). Similarly, the isotopic composition for the net change was calculated according to equation (5) (Table 3).

3.5.2. NO_x, HNO_3^- and p-NO_3^- Flux Measurements

The mean NO_2 concentrations (C_{NO2}) during the campaign were 28.6 ($\sigma = 19.3$) pmol mol^{-1} and 28.7 ($\sigma = 20.3$) pmol mol^{-1} at the upper and lower inlet, respectively (Figure 4a). Similarly, the mean NO concentrations (C_{NO}) were 15.2 ($\sigma = 12.5$) and 16.6 ($\sigma = 17.5$) at the upper and lower inlet respectively (Figure 4b). The C_{NO} and C_{NO2} concentrations showed statistically significant diurnal cycles on some days (9–11, 15–16, and 22–27 April) with amplitudes of 1–36 pmol mol^{-1} and 3–49 pmol mol^{-1} for C_{NO} and C_{NO2}, respectively (Figures 4a and 4b). The diurnal cycles appeared more or less symmetric with UV radiation, with maximum C_{NO} and C_{NO2} observed between 11:00 and 13:00, reaching minima values during nighttime. During periods without diurnal cycles the maximum NO and NO_2 concentrations were reached

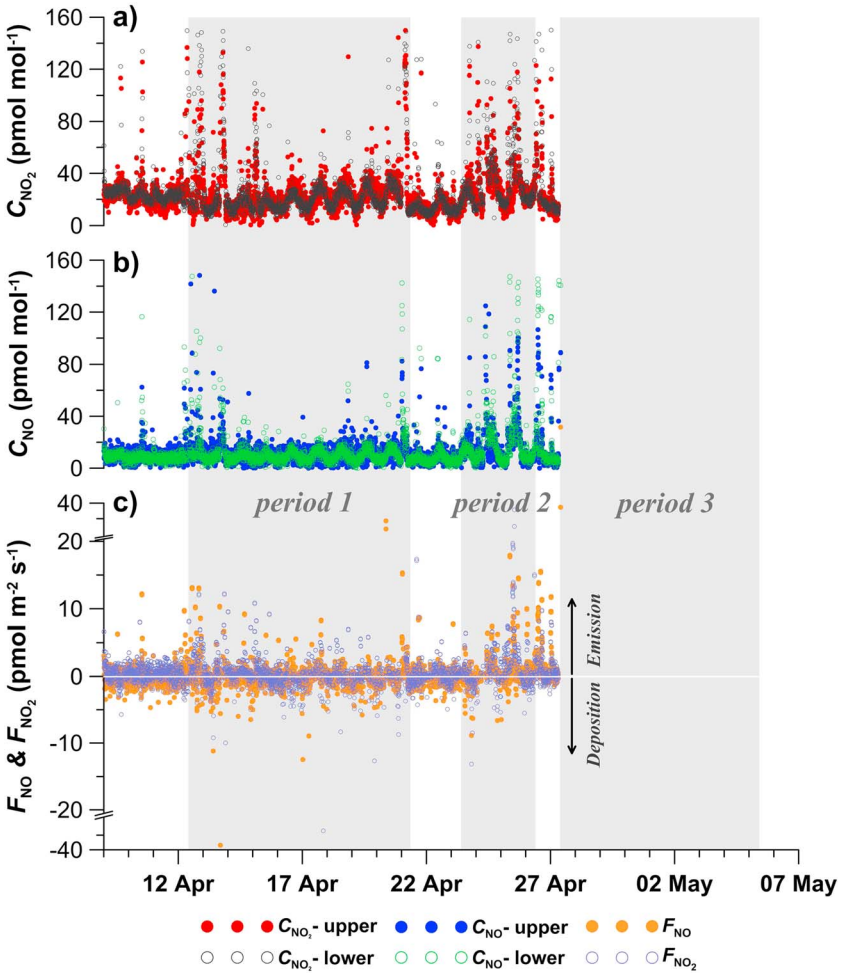

Figure 4. Measured flux data (6 min resolution) from Gruvebadet during the spring campaign 2010, including (a) the NO concentrations (C_{NO}) at the upper and lower inlets; (b) the NO_2 concentrations (C_{NO2}) at the upper and lower inlets; and (c) the NO and NO_2 flux data (F_{NO} and F_{NO2}, respectively) derived from the difference between the upper and lower inlets and the eddy diffusivity, *K*.

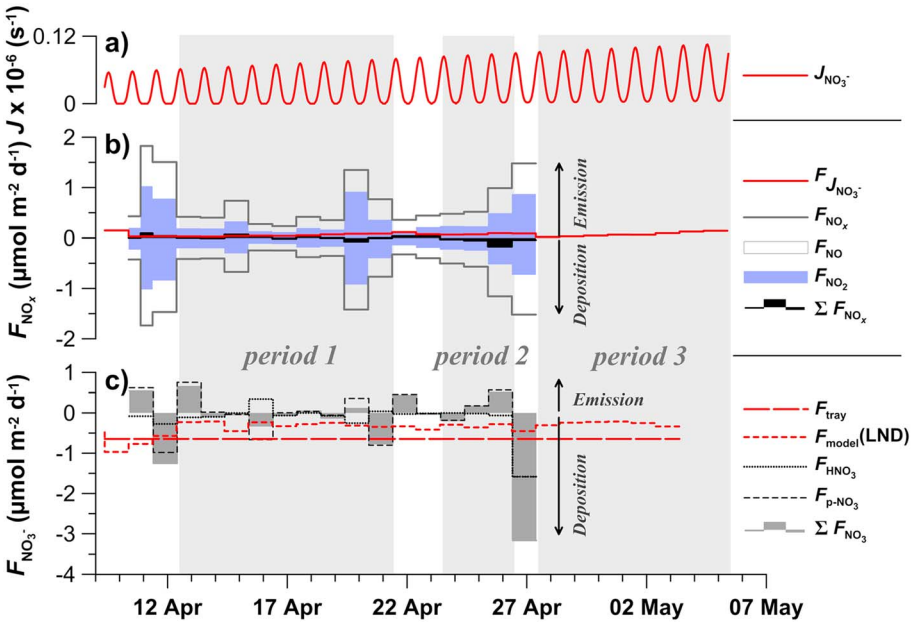

Figure 5. Measured and modeled NO_x, HNO_3, and p-NO_3^- fluxes measured at Gruvebadet. (a) The photolytic rate (J_{NO3-}) estimated from equation (7); (b) the daily average emission and deposition of NO, NO_2, and NO_x (F_{NO}, F_{NO2}, and F_{NOx}) and the daily NO_x net flux (ΣF_{NOx}). Also included is the estimated photolytic NO_2 flux (F_{JNO3-}) using J_{NO3-} in a) and the measured c_{NO3} in Figure 3e; (c) the daily average emission and deposition of HNO_3 (F_{HNO3}) and p-NO_3^- ($F_{p\text{-}NO3}$) and the net flux of these (ΣF_{NO3}), also included is the measured (F_{tray}) and modeled (F_{model}(LND)) NO_3^- dry deposition to Ny-Ålesund given in *Björkman et al*. [2013].

between 18:00 and 21:00, with minimum values measured between 06:00 and 12:00 and, hence, delayed the diurnal irradiance pattern. The turbulence measurements resulted in median eddy diffusivity (K) of 0.2 mol m^{-2} s^{-1} (with the first and third quartile at 0.14 and 0.22 mol m^{-2} s^{-1}, respectively), and the NO_x, HNO_3, and p-NO_3^- fluxes were calculated as K multiplied by the difference between the two inlets (as detailed in *Beine et al*. [2003]). The 6 min NO_x fluxes data (Figure 4c) showed a median NO emission of −0.73 pmol m^{-2} s^{-1} (with the first and third quartile at −0.31 and −1.53 pmol m^{-2} s^{-1}, respectively) with a median NO_2 emission of −0.79 pmol m^{-2} s^{-1} (with the first and third quartile at −0.35 and −1.62 pmol m^{-2} s^{-1}, respectively). The corresponding median NO deposition rates (Figure 4c) were 0.61 pmol m^{-2} s^{-1} (with the first and third quartile at 0.27 and 1.18 pmol m^{-2} s^{-1}, respectively) while the median NO_2 deposition was 0.83 pmol m^{-2} s^{-1} (with the first and third quartile at 0.38 and 1.54 pmol m^{-2} s^{-1}, respectively). The combined daily fluxes of NO_x (F_{NOx}), used for comparison to the surface snow concentrations (Figure 5b), showed an daily averaged F_{NOx} emissions range from −0.2 to −1.8 μmol m^{-2} d^{-1}, and the daily average F_{NOx} depositions ranged from 0.2 to 1.7 μmol m^{-2} d^{-1} (Figure 5b). The resulting daily net fluxes (ΣF_{NOx}) ranged from −0.1 to 0.2 μmol m^{-2} d^{-1} (Figure 5b).

The mean concentrations of HNO_3, fine and coarse particulate NO_3^- were 6.06 ± 5.32, 14.33 ± 13.68, and 15.14 ± 9.53 pmol mol^{-1}, respectively. The HNO_3 and the combined fine and coarse particulate NO_3^- fluxes (F_{HNO3} and $F_{p\text{-}NO3}$, Figure 5c) mostly indicated a deposition, with the mean values of 1.59 ± 1.32 pmol m^{-2} s^{-1} and 4.84 ± 3.52 pmol m^{-2} s^{-1}, respectively. The resulting daily net flux of the total HNO_3 and p-NO_3^- (ΣF_{NO3}) showed variable rates, from −0.6 to 3.2 μmol m^{-2} d^{-1} (Figure 5c), where the flux of p-NO_3^- ($F_{p\text{-}NO3}$) exceeded that of HNO_3 (F_{HNO3}) and thus dominated ΣF_{NO3}, with particularly high rates during the precipitation event between periods 2 and 3 (Figure 5c). The data also show that fine particles (<2.5 μm diameter) were responsible for much of the p-NO_3^- flux during high flux events. The sampling interval (12 or 24 h) for F_{HNO3} and $F_{p\text{-}NO3}$ did not allow a separation of daily emission and deposition estimates, as was achieved using the 6 min F_{NOx} data.

3.6. Box Models

The photolytic rate function (J_{NO3-}) showed clear diurnal variation superimposed upon a uniformly increasing trend (Figure 5a) as a consequence of the steadily rising Sun (midnight Sun commenced on 18 April). The integrated daily surface snow flux (F_{JNO3-}), estimated from J_{NO3-} and c_{NO3}, showed emission rates

of the same order of magnitude as the measured ΣF_{NOx} (Figure 5b). However, $F_{J\ NO3-}$ was considerably lower than the measured NO_x emission (F_{NOx}). This mismatch is likely due to the estimation of NO_3^- photolysis from surface snow only being compared to measured emissions above the full snowpack.

The measured range of the combined HNO_3 and p-NO_3^- fluxes (ΣF_{NO3}) was of the same order of magnitude as the modeled HNO_3 + p-NO_3^- dry deposition (F_{model}(LND)) during this spring campaign [*Björkman et al*., 2013], although the measured average NO_3^- dry deposition (F_{tray}) showed higher spring averages than both F_{model}(LND) and the ΣF_{NO3} (Figure 5c). However, the substantial atmospheric fluxes of HNO_3 and p-NO_3^- (F_{HNO3} and $F_{p\text{-}NO3}$) observed in connection with the precipitation event between periods 2 and 3 was not captured by the dry deposition estimates in *Björkman et al*. [2013] (Figure 5c).

4. Discussion

Here we present a discussion of the trends and influences on NO_3^- concentrations and isotopic composition found for Ny-Ålesund surface snow. We argue that the main process during precipitation-free periods is the addition of NO_3^- through dry deposition, which dominates over NO_3^- postdeposition losses via photolysis and evaporation. However, this dry deposition can be influenced both by atmospheric sources, as well as NO_x, HNO_3^-, and HONO emitted from deeper within the snowpack, processes which therefore require consideration. An active involvement of halogen chemistry was also inferred from the surface snow measurements, and so we discuss the role of surface snow as a contributor in the production of boundary layer BrO.

4.1. Dry Deposition Versus Postdeposition Loss

A striking feature during the spring sampling is the significant increase of c_{NO3} for all three subperiods, in-between precipitation events (Table 1 and Figure 3e), where a positive net change (F_{net}) was confirmed for all periods using equation (2) (Table 3). Hence, equation (2) gives the overall net increase or decrease of c_{NO3}, where the most likely surplus would be due to an NO_3^- addition by dry deposition as long as snow sublimation is low. The measured sublimation rates during the three periods were low and could only have changed the daily c_{NO3} by a modest quantity (average 0.31 ± 0.03%, range 0.2 to 0.8%), which is well below the day to day c_{NO3} variations (average 11.1 ± 1.6%, for the same periods). Similarly, the model photolysis rate ($J_{NO3\text{-}}$) could only have changed the daily c_{NO3} by a 0.2 to 0.4% reduction, indicating a very minor influence of photolysis on these daily variations. Of course, HNO_3 evaporation and HONO emissions could further influence the daily variations. However, both these processes require a surplus of H^+, whereas Ny-Ålesund snow is typically alkaline [*Beine et al*., 2003; *Amoroso et al*., 2006] with a high sea salt content given the close proximity to the fjord. Furthermore, the NO_2^- levels where below the detection limit of the IC measurements (data not shown) further indicating low HONO production. The limited occurrence of sublimation, modeled $J_{NO3\text{-}}$ and positive F_{net} collectively therefore indicate that the addition of NO_3^- through dry deposition outweighed any changes induced by photolytic and/or evaporative loss processes. The estimated F_{net} for the three periods, with a daily weighted average of 0.9 ± 0.4 μmol m^{-2} d^{-1} (Table 3), is also consistent with the measured dry deposition rate (F_{tray}, 0.7 ± 0.3 μmol m^{-2} d^{-1}) estimated for the same time period by *Björkman et al*. [2013]. However, these are slightly higher than the average modeled dry deposition (F_{model}(LND), 0.3 ± 0.1 μmol m^{-2} d^{-1}) for this period [*Björkman et al*., 2013], and also slightly higher than the value *Beine et al*. [2003] found for Ny-Ålesund (~0.2 μmol m^{-2} d^{-1}) during an previous spring, using a diffusion line sampling technique.

The $\delta(^{15}N)$ and $\delta(^{18}O)$ composition of the net change (δ_{net}), as calculated by equation (5), differed between the three subperiods (Table 3). Regarding the F_{net}, no major influence of loss processes was found for periods 1 and 2, since any fractionation during postdeposition loss would have led to an $\delta_{net}(^{15}N)$ increase in NO_3^-. In contrast, periods 1 and 2 showed negative $\delta_{net}(^{15}N)$ values of −8.2 ± 13.6 and −12.2 ± 18.8‰, respectively, even though the validity of these estimates are reduced by the nonsignificant regressions used for calculation. One might argue that the significant positive $\delta_{net}(^{15}N)$ value of (7.0 ± 0.7) ‰ calculated for the NO_3^- in period 3 could be indicative of postdeposition loss. This would, however, contradict the significant c_{NO3} increase and positive F_{net} observed for this period (Table 3), therefore alternative explanations need to be considered, as attempted through box modeling below. The NO_3^- $\delta_{net}(^{18}O)$ found for period 1, even though the linear regression was nonsignificant,

was lower than the isotope delta of the snow (Table 3), whereas for periods 2 and 3 the $\delta_{net}(^{18}O)$ approached the upper limit found for atmospheric HNO_3 in this region (100‰) [*Morin et al*., 2009]. The isotopic signature of snow NO_3^- is, however, influenced by several cooccurring processes as discussed in the section 1 and viewed in Figure 2 and will be further investigated in section 4.3.

4.2. NO_x, HNO_3^-, and p-NO_3^- Flux Measurements

The flux measurements revealed both emissions and deposition fluxes of all the investigated compounds (NO, NO_2, HNO_3^-, and p-NO_3^-, Figures 4 and 5) and where the mean NO and NO_2 concentrations were in agreement with other measurements in the coastal Arctic boundary layer during the same time of year [*Allegrini et al*., 1999; *Beine et al*., 2001, 2002b; *Amoroso et al*., 2010; *Sander and Bottenheim*, 2012]. Although the calculated daily NO and NO_2 fluxes (Figure 5) are in the lower region of what has earlier been reported for Ny-Ålesund by *Amoroso et al*. [2010], the occasional diurnal cycling of NO and NO_2 observed confirms previous studies carried out at Ny-Ålesund [*Beine et al*., 1996, 1997]. Also, the daily average HNO_3 flux measured in 2010 are within the variability of earlier estimates for Ny-Ålesund [*Beine et al*., 2003; *Amoroso et al*., 2010], but substantially lower than the episode with exceptionally high deposition fluxes (up to 1.5 $\mu mol\, m^{-2}\, h^{-1}$) reported by *Amoroso et al*. [2010].

Due to the coastal location of Ny-Ålesund, the chemical composition of snow was dominated by a marine signature. As a result of sea salt inputs, and to a lesser extension of dust, the ionic balance of snow revealed an alkaline character for 44% of the daily snow samples (with pH values between 7.80 and 8.70) which, according to *Beine et al*. [2003, 2008], could lead to a reduced NO_x emission and even to an increased deposition. In addition, it is worth noting that 33% and 41% of all available 6 min NO and NO_2 fluxes (about 5000 values), respectively, indicated a NO_x deposition to the snow surface, as observed in earlier polar studies [e.g., *Beine et al*., 2002; *Amoroso et al*., 2010]. It has previously been shown that the intricate system of NO_3^- photolysis and NO_x emission is followed by a subsequent HNO_3 deposition, producing a diurnal pattern at Summit, Greenland, with daytime emission and nighttime deposition [*Hastings et al*., 2004]. A similar feature can be observed in our 2010 flux data, were the NO and NO_2 emission during periods of high irradiance can be on the same order of magnitude as the total HNO_3 and p-NO_3^- deposition. Indicating that, for this almost alkaline snow environment, the NO_x emissions were reduced or close to zero. Thus, the measured fluxes of NO_x, HNO_3, and p-NO_3^- are neither sufficient to explain the observed c_{NO3} increase. In the following section we will further focus on separating and explaining the processes influencing the surface snow, using the box model to find the most likely sources of the observed NO_3^- deposition and its isotopic signature.

4.3. Reproducing Observed Trends

In the box model used here, describing the main source and sink of NO_3^- in the snow (section 2.4.2), all outgoing fluxes are assumed to be due to photolysis and all incoming fluxes due to HNO_3 dry deposition. As a consequence of the day-to-day variability of isotope deltas and c_{NO3}, our comparison between model and measured data focuses on the regression analysis for the three precipitation-free spring periods, bearing in mind the lower p values for the trends in $\delta(^{15}N)$ and $\delta(^{18}O)$ of snow NO_3^- during periods 1 and 2 (Table 1 and Figure 3).

4.3.1. Box Model Using F_{NOx} and F_{NO3}

The box model (equation (16)) shows that the measured net fluxes of NO_x (ΣF_{NOx}, Figure 5b) and HNO_3 + p-NO_3^- (ΣF_{NO3}, Figure 5c) were insufficient to alter the surface snow c_{NO3} significantly during periods 1 and 2 (Figure 6c, noting the atmospheric flux measurements were terminated on 27 April, just prior to period 3). The small change in c_{NO3} such daily net fluxes would induce was below the detection limit of the snow sampling procedure used here. A similar conclusion was reached by *Beine et al*. [2003] when they compared atmospheric dry deposition estimates with the surface snow NO_3^- concentrations.

In spite of the limited ability of the atmospheric flux driven model to reproduce the surface snow c_{NO3} trends, the modeled influence on $\delta(^{18}O)$ and $\delta(^{15}N)$ was more pronounced (using equation (17), Figure 6). This is especially the case during the first day of period 1, when p-NO_3^- emission (Figure 5c) resulted in an increased modeled $\delta(^{18}O)$, and where the $\delta_{atm}(^{18}O)$ scenarios +40 and +100‰ followed the very lower and upper limit of the data variability for the rest of period 1 (Figure 6a). Although particle emission from

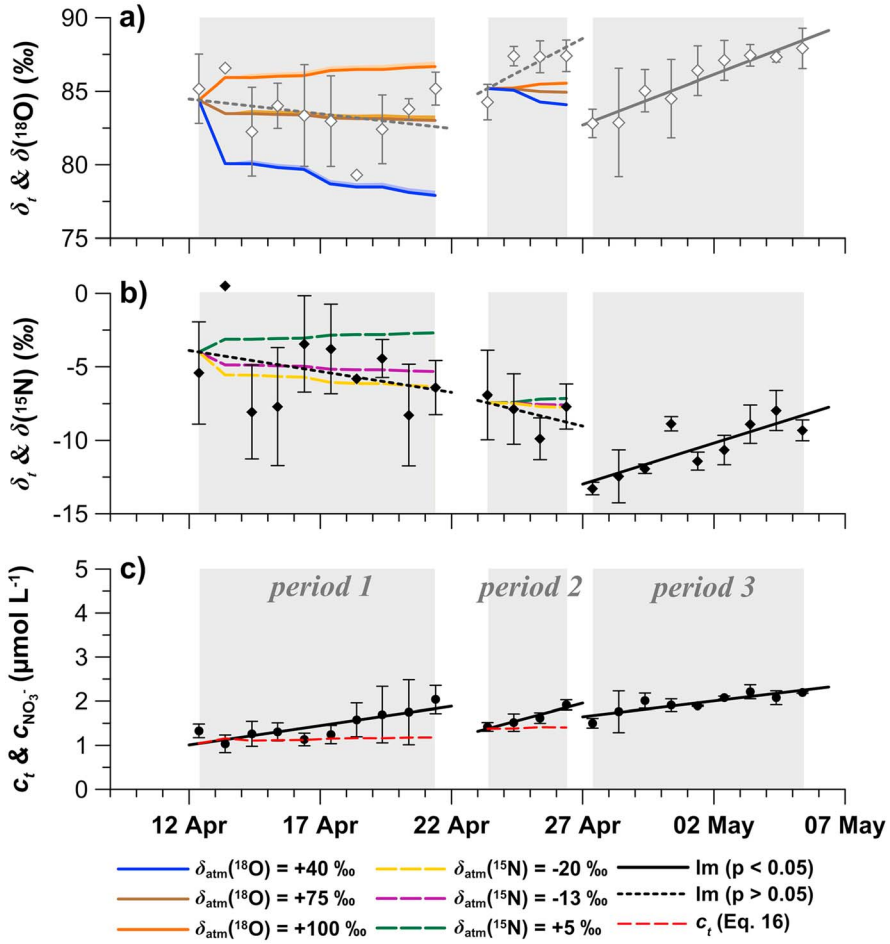

Figure 6. Box model results, using the NO_x, HNO_3^-, and p-NO_3^- flux measurements. (a) The modeled δ_t for ^{18}O (equation (13)) for the three isotopic deposition scenarios (δ_{atm}), where +40‰ resembles the OH signal found in Greenland [*Jarvis et al.*, 2009], +75‰ resembles a midlatitude signal [*Morin et al.*, 2009], and +100‰ resembles the influence of BrO chemistry [*Morin et al.*, 2009]. Also included in Figure 6a is the actual measured $\delta(^{18}O)$ and cooccurring linear regression models (lm, Table 1). (b)The modeled δ_t for ^{15}N (equation (13)) for the three isotopic deposition scenarios (δ_{atm}), where −20‰ represents polar basin air [*Morin et al.*, 2009], −13‰ represent ambient air [*Amoroso et al.*, 2010], and +5‰ represents a local biogeochemical signal [*Amoroso et al.*, 2010]. Also included in Figure 6b is the measured $\delta(^{15}N)$ and developed lm's. (c) The modeled c_t (equation (16)) along with the measured c_{NO3} and lm's. Furthermore, the fractionation sensitivity test is included as shaded areas around the box model results in Figures 6a and 6b.

snow might be limited [*Cadle*, 1991], some resuspension of particles by wind is possible [*Barrie et al.*, 1998]. During period 2 neither of the $\delta_{atm}(^{18}O)$ scenarios followed the observed $\delta(^{18}O)$ pattern. For periods 1 and 2, the modeled d^{15}N was not as sensitive to the choice of $\delta_{atm}(^{15}N)$ scenarios (+5, −13, and −20‰), as for $\delta(^{18}O)$. In fact, model results for all three $\delta_{atm}(^{15}N)$ scenarios were well within the data variability and did not deviate much from each other (Figure 6b). Overall, none of the δ_{atm} scenarios and emission fractionations, including the sensitivity test for different fractionations ($^{15}\varepsilon$ and $^{18}\varepsilon$, section 2.4.2), reproduced the observed trends in a satisfactory way. This is probably due to the many layers found in the sampled surface snow during period 1 and 2, that can yield large daily variations in $\delta(^{15}N)$ and $\delta(^{18}O)$. It is especially troublesome that the observed c_{NO3} trends (Table 1) and calculated dry deposition rates (Table 3) cannot be explained by the atmospheric flux in the box model. A possible explanation could be a redeposition of NO_x, HNO_3^-, and HONO emitted from deeper within the snowpack, or the soil below, to the surface snow layer. Such a subsurface source would then not necessarily need to involve an emission to the atmospheric boundary layer, thus could impact the surface snow measurements of NO_3^- deposition but not the atmospheric flux measurements as a result.

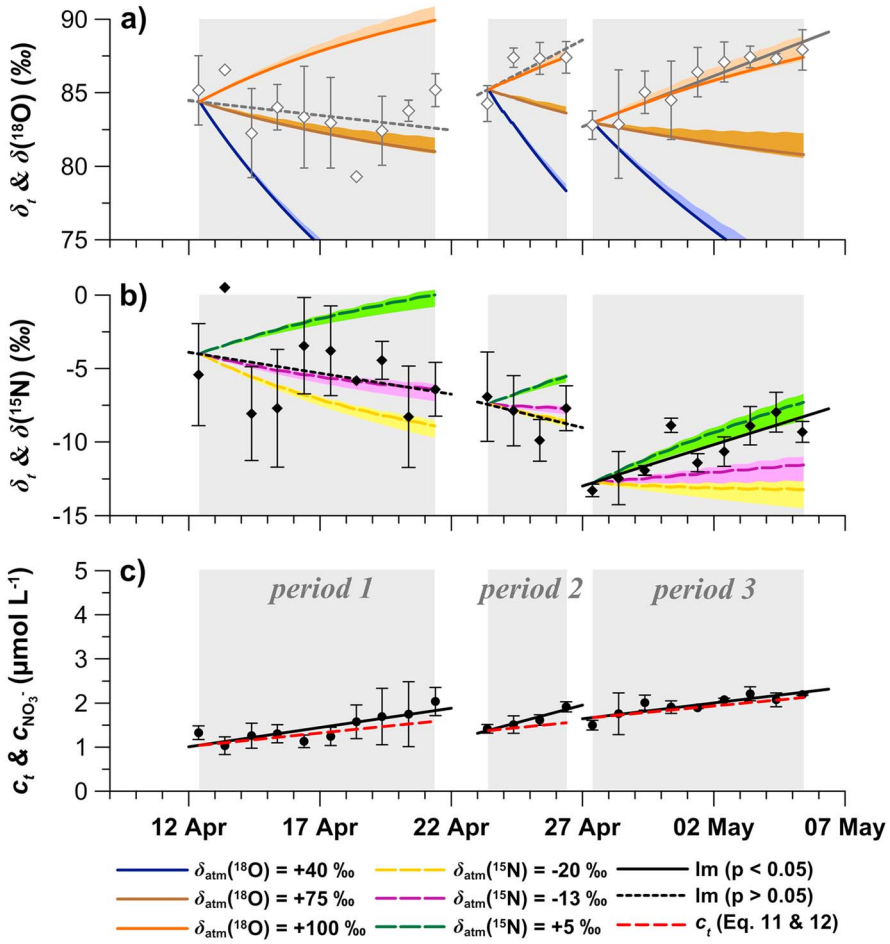

Figure 7. Same as Figure 6 but where the box model parameterization for the emission of NO_x is based on the photolytic rate function (J_{NO3^-}, equation (7)) and the deposition of NO_3^- from the atmosphere based on the dry deposition rate (F_{tray}) using equations (11) and (12).

4.3.2. Box Model Using J_{NO3^-} and F_{model}(LND) or F_{tray}

As a second attempt to reproduce the observed surface snow trends (equations (11) and (12)) and to also address the observations of period 3, which can be considered most reliable as the surface snow was one homogeneous layer, the modeled photolysis (J_{NO3-}) was used in conjunction with F_{model}(LND), Figure S2. This box modeling attempt, and a third approach, using J_{NO3-} in conjunction with F_{tray}, Figure 7, captured the c_{NO3} trends far better than the atmospheric flux measurements. This was particularly the case with the third attempt, which reproduced the observed c_{NO3} increase during period 3 in a sufficient manner (Figure 7c), attributing the addition through dry deposition to have a prevailing role over photolytic and, probably, evaporative loss.

For the isotopic composition the models (equations (14) and (15)) seems to have had a clear negative influence upon the surface $\delta(^{15}N)$ signature during periods 1 and 2 (Figures S2 and 7), with a $\delta_{atm}(^{15}N)$ close to the ambient atmospheric (−13‰) [*Amoroso et al.*, 2010] and the Polar Basin signals (−20‰) [*Morin et al.*, 2009]. This also corresponds well to the main back trajectories observed during these periods (Figure 3c). In contrast, period 3 indicated the influence of a positive end-member (+7.0 ± 0.7‰, Table 3) that cannot be explained by a photolytic and/or evaporative NO_3^- loss, hence indicates dry deposition seems to have occurred. This positive $\delta(^{15}N)$ signature is more in line with the +5‰ previously described for snowpack biogeochemical processes in this region [*Amoroso et al.*, 2010], indicating a redeposition of NO_x, HNO_3^-, and HONO emitted deeper within (or below) the snowpack. However, anthropogenic NO_x emissions are also in general slightly positive [e.g., *Hastings*, 2010], with the exception of agricultural soils [*Felix and Elliott*, 2013]. For example, *Morin et al.* [2009] found an atmospheric nitrate signal of +5.9‰ from European air in the English Channel, a value also consistent with midlatitude spring values for the U.S. [*Elliott et al.*, 2009]. For

period 3, the air mass back trajectories are more stagnant around Svalbard, with a southeasterly influence at the end of this period. This indicates that the high end-member found for period 3 could also be influenced by local or European emission sources, and is not necessarily solely a biogeochemical signal.

For period 1, the $\delta(^{18}O)$ end-member is close to the midlatitude scenario (+75‰, Figures S2 and 7), which is also the post-1950 background value for this region as indicated by Svalbard ice core averages (+75.1 ± 4.1‰) [*Vega*, 2014], in spite of a northerly airflow which was assumed to bring a $\delta(^{18}O)$ signal around +100‰. The $\delta(^{18}O)$ end-member for periods 2 and 3 is on the other hand more in line with air masses from the Polar Basin [*Morin et al*., 2009], for which the uniquely high $\delta(^{18}O)$ has been found to result from an active atmospheric BrO interaction (Figure 2) [*Morin et al*., 2007a, 2007b]. This is especially surprising for period 3, where the back trajectories are stagnant or southeasterly oriented, with only a minor influence of Polar air (Figure 3c). Under these circumstances a midlatitude $\delta(^{18}O)$ scenario would be expected for period 3, rather than the +100‰ evidenced here. The reason for this deviation is probably due to a local snow-determined BrO-NO_x interaction, the first such observation of its kind in this region, and will be further discussed in section 4.

The sensitivity test performed (shaded ranges in Figures 6, 7, and S2) indicates that the actual photolytic fractionation used in the box modeling has little influence on the outcome, probably due to the prevailing dry deposition regime in our surface snow.

In summary, period 1 shows evidence of a polar basin/ ambient atmospheric influence on $\delta(^{15}N)$ and a $\delta(^{18}O)$ signature that resembles midlatitudinal air. Period 2 shows a polar basin influence upon both the $\delta(^{15}N)$ and the $\delta(^{18}O)$ signatures; while period 3 has a $\delta(^{15}N)$ similar to that which is expected from either biogeochemical cycling of NH_4^+ in the snowpack, or local/European emissions, along with the BrO influenced $\delta(^{18}O)$ signature.

4.4. O_3 and BrO Interaction

During the spring campaign several O_3 depletion events (ODE) occurred; on 13, 21–22, 26–27, and 30 April to 1 May (Figure 3b). Such events are known in the Arctic as a result of active halogen chemistry where Br_2, BrCl, or Cl_2 (ultimately of oceanic origin, whose release is believed to involve snow and first-year sea ice) are released in to the boundary layer. Their rapid photolysis by solar radiation forms Br or Cl radicals, which then initiates a chain reaction depleting O_3 (Figure 2) [e.g., *Foster et al*., 2001; *Simpson et al*., 2007; *Abbatt et al*., 2012]. For Ny-Ålesund, studies typically observe such events as a consequence of the advection of air masses already depleted in O_3, originating from the polar basin [e.g., *Barrie and Platt*, 1997], where low levels of boundary layer O_3 are typical during spring [*Hopper et al*., 1994, 1998; *Jacobi et al*., 2010]. This is consistent with the ODEs observed during the spring 2010, where more northerly air flows occur prior to the ozone depletion episodes (Figure 3) and where satellite data [*Begoin et al*., 2010] reveals increased BrO column abundances concurrent with the ODE's (Figure S3). Alongside its impact on boundary layer O_3, BrO can also influence NO_x cycling and its transformation to HNO_3, via the formation and hydrolysis of $BrONO_2$. This generates a uniquely high $\delta(^{18}O)$ (Figure 2) [e.g., *Evans et al*., 2003; *Morin et al*., 2007b].

For period 2 a northerly airflow was observed which can explain both the low $\delta(^{15}N)$ (photolytic produced NO_x from polar basin snowpacks) and the high $\delta(^{18}O)$ (BrO pathway) end-member [*Morin et al*., 2009]. However, for period 3, when the airflow is stagnant or southwesterly, with only a minor influence of polar basin air, the high $\delta(^{18}O)$ end-member would need to have another explanation. Interestingly, the Br^- concentrations (c_{Br}) in the surface snow are high during period 1, decrease during period 2, then remain low and slightly decrease further during period 3 (Figure 3b and Table 1). There is also a significant ($p < 0.05$) negative correlation between the daily averages of c_{Br} and c_{NO3} ($R = -0.84$) during period 3, as well as between c_{Br} and $\delta(^{15}N)$ and $\delta(^{18}O)$ ($R = -0.91$ and -0.83, respectively). According to the BrO pathway in Figure 2, formation of $BrONO_2$ from $BrO + NO_2$ can be followed by a photolytic dissociation, or—particularly under conditions of high surface area—be followed by hydrolysis whereby $BrONO_2$ disintegrates into HNO_3 and HOBr on ice crystals [*Evans et al*., 2003; *Morin et al*., 2007b]. This latter case thereby converts NO_x into HNO_3. Assuming that this reaction occurs within the snow or just above, the newly formed HOBr would further react with Br^- ions in the DI with a release of gaseous Br_2 as a result [e.g., *Simpson et al*., 2007; *Abbatt et al*., 2012]. In the presence of a NO_x, HNO_3, or HONO supply from deeper within the snowpack (i.e., photolysis, evaporation, or biologic emissions from the snow or soil), this BrO-NO_x chemistry would rapidly redeposit the NO_x as HNO_3 in the surface snow. This would then minimize any snowpack emissions and, in the

case of negligible local soil emissions, keep the total snow NO_3^- budget unaltered. This coupled BrO-NO_x chemistry can explain both the decrease in Br^- concentration in the surface snow as well as the increasing $\delta(^{18}O)$ and c_{NO3} values observed in the surface snow during periods 2 and 3. This is the first time such coupling has been observed in Svalbard, although increasing BrO levels have earlier been reported above Ny-Ålesund snow following an ODE [*Avallone et al*., 2003]. To start the BrO production and following chain reactions, an initial pulse (or "seed") of reactive halogens is needed [*Simpson et al*., 2007]. It is however, unlikely that the BrO cycling seen in our c_{Br} and $\delta(^{18}O)$ data, and in the BrO record from *Avallone et al*. [2003] are initiated locally. They are likely rather results of polar basin air advection providing seed halogens during the observed ODEs, which then initiate the local BrO production. This hypothesis is further strengthened by the column content of BrO (Figure S3) where the atmosphere above western Svalbard, and eastern parts of the Fram Strait, shows prevailing low BrO levels, which only increases in conjunction with ODE's when surges of BrO moves into the Ny-Ålesund area. Nevertheless, during period 3, our surface snow bromide, nitrate, and $\delta(^{18}O)$ observations provide evidence for continued local (snowpack) BrO-NO_x cycling, even while BrO column abundances decline and ambient air ozone recovers.

5. Conclusion

Detailed sampling of the photoactive surface zone of the Ny-Ålesund snowpack during winter and springtime demonstrates that NO_3^- dry deposition is the predominant process determining NO_3^- concentrations during precipitation-free periods and prevails over any NO_3^- postdeposition loss via photolysis and HNO_3 evaporation within this layer. The measured dry deposition in uniform surface snow ($0.6 \pm 0.2\ \mu mol\ m^{-2}\ d^{-1}$) is in line with previously reported values for Ny-Ålesund [*Björkman et al*., 2013]. However, it indicates greater net deposition than that derived from cumulative NO_x, HNO_3^-, and p-NO_3^- fluxes, measured 200 m from the sampling site. Given its permeable nature, we emphasize that the snowpack should be considered as an integral part of the atmospheric boundary layer, allowing relevant reactions (Figure 2) to occur within interstitial air pockets within the snow. Thus, our observed dry deposition of NO_3^- could originate from both the overlying atmosphere and from redeposition of NO_3^- released from deeper within the snowpack or soil below.

Magnitudes and trends in surface snow $\delta(^{15}N)$ and $\delta(^{18}O)$ were compared to back trajectory analysis and local ODEs indicative of BrO chemistry. Trajectories originating from the polar basin were found to bring ^{15}N-depleted air masses to Svalbard, confirming findings from an earlier atmospheric study of NO_3^- in Ny-Ålesund aerosol [*Morin et al*., 2009], and demonstrating that such NO_3^- is deposited to the snowpack. Stagnant air and air masses originating from midlatitude regions were related to ^{15}N-enriched dry NO_3^- deposition with an end-member of $(+7.0 \pm 0.7)‰$. Such positive $\delta(^{15}N)$ values have previously been found in European and U.S. air [*Elliott et al*., 2009; *Morin et al*., 2009], probably as a result of anthropogenic emissions [e.g., *Kendall et al*., 2007], but can also result from in situ biogeochemical cycling of clay-bound NH_4^+ [*Amoroso et al*., 2010].

The average $\delta(^{18}O)$ values were lower during the wintertime compared to springtime, when NO_3^- deposition from polar basin air masses only exhibited positive $\delta(^{18}O)$ trends in conjunction with low O_3 levels. These conditions indicate active halogen cycling and demonstrate the importance of NO_x to NO_3^- formation via coupled BrO-NO_x chemistry (as identified in Ny-Ålesund aerosol: *Morin et al*. [2009]) for snow NO_3^- deposition. Furthermore, we identify evidence for such BrO chemistry occurring within the snowpack (interstitial air pockets) itself, and demonstrate its active involvement in the NO_3^- postdeposition cycling, as evidenced by steadily decreasing snow Br^- content and increasing $\delta(^{18}O)$ and NO_3^- concentration in surface snow samples. These are the first observations of such snowpack BrO-NO_x coupling in this part of the Arctic. However, as indicated both by this and a previous study [*Avallone et al*., 2003], local BrO production is concomitant with the arrival of BrO active O_3-depleted air, which contributes the necessary seed halogens to get the local production initiated [*Simpson et al*., 2007]. This production might explain the uniquely high $\delta(^{18}O)$ end-member $(+105.9 \pm 72.3‰)$ found even during stagnant and southeasterly air influences, regions usually associated with higher O_3 levels.

In summary, our study demonstrates how careful sampling of surface snow can provide useful insights regarding atmospheric and snow processes controlling the fate of reactive nitrogen in the Arctic including coupling of BrO-NO_x chemistry. In particular, our results elucidate the relative importance of these processes for a snowpack located in a coastal region at low altitude (Ny-Ålesund), in contrast to studies elsewhere (e.g., Greenland).

Acknowledgments

This work was part of the international project *Sources, sinks and impacts of atmospheric nitrogen deposition in the Arctic* (NSINK) and received financial support from the EU Marie Curie Initial Stage Training Network Award (NSINK, FP7 215503). Fieldwork was supported by Arctic Field Grant, Svalbard Science Forum. This work is also a contribution to *Cryosphere-Atmosphere interaction in a changing arctic climate* (*CRAICC*) a Top-Level Research Initiative (TRI). TJR acknowledges LABEX VOLTAIRE (VOLatils-Terre Atmosphère Interactions-Ressources et Environnement) ANR-10-LABX-100-01 (2011–20). Logistic support was provided by the staff at the Sverdrup Station, Norwegian Polar Institute. NILU. is acknowledged for providing the FLEXTRA trajectories and Zeppelin O_3 data, wears DNMI for providing meteorological data. The authors are grateful for the support from Mauro Mazzola and Angelo Viola (ISCA-CNR) for providing water vapor flux data and from Andreas Richter (University of Bremen) contributing with the supplementary BrO maps. This manuscript has also been improved by comments from three anonymous reviewers.

References

Abbatt, J. P. D. (1997), Interaction of HNO_3 with water-ice surfaces at temperatures of the free troposphere, *Geophys. Res. Lett.*, *24*, 1479–1482, doi:10.1029/97GL01403.

Abbatt, J. P. D., et al. (2012), Halogen activation via interactions with environmental ice and snow in the polar lower troposphere and other regions, *Atmos. Chem. Phys.*, *12*, 6237–6271.

Albert, M. R., and J. P. Hardy (1995), Ventilation experiments in a seasonal snow cover, in *Biogeochemistry of Seasonally Snow-Covered Catchments*, edited by K. A. Tonnessen, pp. 41–49, Int. Assoc. of Hydrol. Sci., Wallingford, U. K.

Albert, M. R., A. M. Grannas, J. Bottenheim, P. B. Shepson, and F. E. Perron (2002), Processes and properties of snow-air transfer in the high Arctic with application to interstitial ozone at Alert, Canada, *Atmos. Environ.*, *36*, 2779–2787.

Allegrini, I., A. Ianniello, M. Montagnoli, R. Sparapani, M. Gomez, and C. de Teran (1999), Carbon-coated annular denuders and ion chromatographic measurements for the determination of nitrogen-containing species (NO_2 and NO_y) in remote atmospheres, *J. Chromatogr., A*, *846*, 265–268.

Amato, P., R. Hennebelle, O. Magand, M. Sancelme, A. M. Delort, C. Barbante, C. Boutron, and C. Ferrari (2007), Bacterial characterization of the snow cover at Spitzberg, Svalbard, *Fems Microbiol. Ecol.*, *59*, 255–264.

Amoroso, A., H. J. Beine, R. Sparapani, M. Nardino, and I. Allegrini (2006), Observation of coinciding Arctic boundary layer ozone depletion and snow surface emissions of nitrous acid, *Atmos. Environ.*, *40*, 1949–1956.

Amoroso, A., et al. (2010), Microorganisms in dry polar snow are involved in the exchanges of reactive nitrogen species with the atmosphere, *Environ. Sci. Technol.*, *44*, 714–719.

Avallone, L. M., D. W. Toohey, T. J. Fortin, K. A. McKinney, and J. D. Fuentes (2003), In situ measurements of bromine oxide at two high-latitude boundary layer sites: Implications of variability, *J. Geophys. Res.*, *108*(D3), 4089, doi:10.1029/2002JD002843.

Barrie, L., and U. Platt (1997), Arctic tropospheric chemistry: An overview, *Tellus Ser. B*, *49*, 450–454.

Barrie, L., E. Falck, D. J. Gregor, T. Iversen, H. Loeng, R. Macdonald, S. Pfirman, T. Skotvold, and E. Wartena (1998), The influence of physical and chemical processes on contaminant transport into and within the Arctic, in *AMAP Assessment Report: Arctic Pollution Issues*, edited by D. J. Gregor, H. Loeng, and L. Barrie, pp. 25–116, Arctic Monitoring and Assessment Programme (AMAP), Oslo.

Bartels-Rausch, T., et al. (2012), A review of air-ice chemical and physical interactions (AICI): Liquids, quasi-liquids, and solids in snow, *Atmos. Chem. Phys.*, *14*, 1587–1633.

Begoin, M., A. Richter, M. Weber, L. Kaleschke, X. Tian-Kunze, A. Stohl, N. Theys, and J. P. Burrows (2010), Satellite observations of long range transport of a large BrO plume in the Arctic, *Atmos. Chem. Phys.*, *10*, 6515–6526.

Beine, H. J., M. Engardt, D. A. Jaffe, Ø. Hov, K. Holmén, and F. Stordal (1996), Measurements of NO_x and aerosol particles at Ny-Ålesund Zeppelin mountain station on Svalbard: Influence of regional and local pollution sources, *Atmos. Environ.*, *30*, 1067–1079.

Beine, H. J., D. A. Jaffe, J. A. Herring, J. A. Kelley, T. Krognes, and F. Stordal (1997), High-latitude springtime photochemistry. Part 1. NO_x, PAN and ozone relationships, *J. Atmos. Chem.*, *27*, 127–153.

Beine, H. J., I. Allegrini, R. Sparapani, A. Ianniello, and F. Valentini (2001), Three years of springtime trace gas and particle measurements at Ny-Alesund, Svalbard, *Atmos. Environ.*, *35*, 3645–3658.

Beine, H. J., F. Domine, W. Simpson, R. E. Honrath, R. Sparapani, X. L. Zhou, and M. King (2002a), Snow-pile and chamber experiments during the Polar Sunrise Experiment "Alert 2000": Exploration of nitrogen chemistry, *Atmos. Environ.*, *36*, 2707–2719.

Beine, H. J., R. E. Honrath, F. Domine, W. R. Simpson, and J. D. Fuentes (2002b), NO_x during background and ozone depletion periods at Alert: Fluxes above the snow surface, *J. Geophys. Res.*, *107*(D21), 4584, doi:10.1029/2002JD002082.

Beine, H. J., F. Domine, A. Ianniello, M. Nardino, I. Allegrini, K. Teinilä, and R. Hillamo (2003), Fluxes of nitrates between snow surfaces and the atmosphere in the European high Arctic, *Atmos. Chem. Phys.*, *3*, 335–346.

Beine, H., A. J. Colussi, A. Amoroso, G. Esposito, M. Montagnoli, and M. R. Hoffmann (2008), HONO emissions from snow surfaces, *Environ. Res. Lett.*, *3*, doi:10.1088/1748-9326/3/4/045005.

Bergin, M. H., J. L. Jaffrezo, C. I. Davidson, J. E. Dibb, S. N. Pandis, R. Hillamo, W. Maenhaut, H. D. Kuhns, and T. Makela (1995), The contributions of snow, fog, and dry deposition to the summer flux of anions and cations at Summit, Greenland, *J. Geophys. Res.*, *100*, 16,275–16,288, doi:10.1029/95JD01267.

Björkman, M. P., R. Kühnel, D. G. Partridge, T. J. Roberts, W. Aas, M. Mazzola, A. Viola, A. Hodson, J. Ström, and E. Isaksson (2013), Nitrate dry deposition in Svalbard, *Tellus, Ser. B*, *65*, doi:10.3402/tellusb.v65i0.19071.

Blunier, T., G. L. Floch, H. W. Jacobi, and E. Quansah (2005), Isotopic view on nitrate loss in Antarctic surface snow, *Geophys. Res. Lett.*, *32*, L13501, doi:10.1029/2005GL023011.

Boxe, C. S., and A. Saiz-Lopez (2008), Multiphase modeling of nitrate photochemistry in the quasi-liquid layer (QLL): Implications for NO_x release from the Arctic and coastal Antarctic snowpack, *Atmos. Chem. Phys.*, *8*, 4855–4864.

Brooks, P. D., S. K. Schmidt, and M. W. Williams (1997), Winter production of CO_2 and N_2O from Alpine tundra: Environmental controls and relationship to inter-system C and N fluxes, *Oecologia*, *110*, 403–413.

Cadle, S. H. (1991), Dry deposition to Snowpacks, in *Seasonal Snowpacks*, edited by T. D. Davies, M. Tranter, and H. G. Jones, pp. 21–66, Springer, Berlin.

Cadle, S. H., J. M. Dasch, and P. A. Mulawa (1985), Atmospheric concentrations and the deposition velocity to snow of nitric-acid, sulfur-dioxide and various particulate species, *Atmos. Environ.*, *19*, 1819–1827.

Chu, L., and C. Anastasio (2003), Quantum yields of hydroxyl radical and nitrogen dioxide from the photolysis of nitrate on ice, *J. Phys. Chem. A*, *107*, 9594–9602.

Colbeck, S. C. (1997), Model of wind pumping for layered snow, *J. Glaciol.*, *43*, 60–65.

Coplen, T. B., J. K. Bohke, and K. L. Casciotti (2004), Using dual-bacterial denitrification to improve $\delta^{15}N$ determinations of nitrates containing mass-independent ^{17}O, *Rapid Commun. Mass Spectrom.*, *18*, 245–250.

Cress, R. G., M. W. Williams, and H. Sievering (1995), Dry depositional loading of nitrogen to an alpine snowpack, Niwot Ridge, Colorado, *Biogeochem. Seasonally Snow-Covered Catchments*, *IAHS Publ. no. 228*, 33–40.

Dentener, F. J., and P. J. Crutzen (1993), Reaction of N_2O_5 on tropospheric aerosols—Impact on the global distributions of NO_x, O_3, and OH, *J. Geophys. Res.*, *98*, 7149–7163, doi:10.1029/92JD02979.

Dibb, J. E., R. W. Talbot, J. W. Munger, D. J. Jacob, and S. M. Fan (1998), Air-snow exchange of HNO_3 and NO_y at Summit, Greenland, *J. Geophys. Res.*, *103*, 3475–3486, doi:10.1029/97JD03132.

Dickerson, R. R. (1985), Reactive nitrogen-compounds in the Arctic, *J. Geophys. Res.*, *90*, 10,739–10,743, doi:10.1029/JD090iD06p10739.

Diehl, K., S. K. Mitra, and H. R. Pruppacher (1995), A laboratory study of the uptake of HNO_3 and HCL vapor by snow crystals and ice spheres at temperatures between 0 and −40°C, *Atmos. Environ.*, *29*, 975–981.

Domine, F., and P. B. Shepson (2002), Air-snow interactions and atmospheric chemistry, *Science*, *297*, 1506–1510.
Domine, F., M. Albert, T. Huthwelker, H. W. Jacobi, A. A. Kokhanovsky, M. Lehning, G. Picard, and W. R. Simpson (2008), Snow physics as relevant to snow photochemistry, *Atmos. Chem. Phys.*, *8*, 171–208.
Elliott, E. M., C. Kendall, E. W. Boyer, D. A. Burns, G. G. Lear, H. E. Golden, K. Harlin, A. Bytnerowicz, T. J. Butler, and R. Glatz (2009), Dual nitrate isotopes in dry deposition: Utility for partitioning NOx source contributions to landscape nitrogen deposition, *J. Geophys. Res.*, *114*, G04020, doi:10.1029/2008JG000889.
Erbland, J., W. C. Vicars, J. Savarino, S. Morin, M. M. Frey, D. Frosini, E. Vince, and J. M. F. Martins (2013), Air-snow transfer of nitrate on the East Antarctic Plateau—Part 1: Isotopic evidence for a photolytically driven dynamic equilibrium, *Atmos. Chem. Phys.*, *13*, 6403–6419.
Evans, M. J., et al. (2003), Coupled evolution of BrO_x-ClO_x-HO_x-NO_x chemistry during bromine-catalyzed ozone depletion events in the arctic boundary layer, *J. Geophys. Res.*, *108*(D4), 8368, doi:10.1029/2002JD002732.
Febo, A., F. Desantis, C. Perrino, and M. Giusto (1989), Evaluation of laboratory and field performance of denuder tubes—A theoretical approach, *Atmos. Environ.*, *23*, 1517–1530.
Felix, J. D., and E. M. Elliott (2013), The agricultural history of human-nitrogen interactions as recorded in ice core $\delta^{15}N\text{-}NO_3^-$, *Geophys. Res. Lett.*, *40*, 1642–1646, doi:10.1002/grl.50209.
Foster, K. L., R. A. Plastridge, J. W. Bottenheim, P. B. Shepson, B. J. Finlayson-Pitts, and C. W. Spicer (2001), The role of Br_2 and BrCl in surface ozone destruction at polar sunrise, *Science*, *291*, 471–474.
France, J. L., M. D. King, and J. Lee-Taylor (2010), The importance of considering depth-resolved photochemistry in snow: A radiative-transfer study of NO_2 and OH production in Ny-Alesund (Svalbard) snowpacks, *J. Glaciol.*, *56*, 655–663.
France, J. L., M. D. King, M. M. Frey, J. Erbland, G. Picard, S. Preunkert, A. MacArthur, and J. Savarino (2011a), Snow optical properties at Dome C (Concordia), Antarctica: Implications for snow emissions and snow chemistry of reactive nitrogen, *Atmos. Chem. Phys.*, *11*, 9787–9801.
France, J. L., M. D. King, J. Lee-Taylor, H. J. Beine, A. Ianniello, F. Domine, and A. MacArthur (2011b), Calculations of in-snow NO_2 and OH radical photochemical production and photolysis rates: A field and radiative-transfer study of the optical properties of Arctic (Ny-Alesund, Svalbard) snow, *J. Geophys. Res.*, *116*, F04013, doi:10.1029/2011JF002019.
Frey, M. M., R. W. Stewart, J. R. McConnell, and R. C. Bales (2005), Atmospheric hydroperoxides in West Antarctica: Links to stratospheric ozone and atmospheric oxidation capacity, *J. Geophys. Res.*, *110*, D23301, doi:10.1029/2005JD006110.
Frey, M. M., J. Savarino, S. Morin, J. Erbland, and J. M. F. Martins (2009), Photolysis imprint in the nitrate stable isotope signal in snow and atmosphere of East Antarctica and implications for reactive nitrogen cycling, *Atmos. Chem. Phys.*, *9*, 8681–8696.
Freyer, H. D. (1991), Seasonal variation of $^{15}N/^{14}N$ ratios in atmospheric nitrate species, *Tellus Ser. B-Chem. Phys. Meteorol.*, *43*, 30–44.
Galbavy, E. S., C. Anastasio, B. Lefer, and S. Hall (2007), Light penetration in the snowpack at Summit, Greenland: Part 2 nitrate photolysis, *Atmos. Environ.*, *41*, 5091–5100.
Grannas, A. M., et al. (2007), An overview of snow photochemistry: Evidence, mechanisms and impacts, *Atmos. Chem. Phys.*, *7*, 4329–4373.
Hanson, D. R., and A. R. Ravishankara (1995), Heterogeneous chemistry of bromine species in sulfuric-acid under stratospheric conditions, *Geophys. Res. Lett.*, *22*, 385–388, doi:10.1029/94GL03379.
Hanson, D. R., A. R. Ravishankara, and E. R. Lovejoy (1996), Reaction of $BrONO_2$ with H_2O on submicron sulfuric acid aerosol and the implications for the lower stratosphere, *J. Geophys. Res.*, *101*, 9063–9069, doi:10.1029/96JD00347.
Hastings, M. G. (2010), Evaluating source, chemistry and climate change based upon the isotopic composition of nitrate in ice cores, *IOP Conf. Ser. Earth Environ. Sci.*, *9*, 012002, doi:10.1088/1755-1315/9/1/012002.
Hastings, M. G., E. J. Steig, and D. M. Sigman (2004), Seasonal variations in N and O isotopes of nitrate in snow at Summit, Greenland: Implications for the study of nitrate in snow and ice cores, *J. Geophys. Res.*, *109*, D20306, doi:10.1029/2004JD004991.
Hirdman, D., H. Sodemann, S. Eckhardt, J. F. Burkhart, A. Jefferson, T. Mefford, P. K. Quinn, S. Sharma, J. Ström, and A. Stohl (2010), Source identification of short-lived air pollutants in the Arctic using statistical analysis of measurement data and particle dispersion model output, *Atmos. Chem. Phys.*, *10*, 669–693.
Hodson, A. J., P. N. Mumford, J. Kohler, and P. M. Wynn (2005), The High Arctic glacial ecosystem: New insights from nutrient budgets, *Biogeochemistry*, *72*, 233–256.
Hodson, A. J., T. J. Roberts, A.-C. Engvall, K. Holmén, and P. Mumford (2010), Glacier ecosystem response to episodic nitrogen enrichment in Svalbard, European High Arctic, *Biogeochemistry*, *98*(1–3), 171–184.
Honrath, R. E., M. C. Peterson, S. Guo, J. E. Dibb, P. B. Shepson, and B. Campbell (1999), Evidence of NO_x production within or upon ice particles in the Greenland snowpack, *Geophys. Res. Lett.*, *26*, 695–698, doi:10.1029/1999GL900077.
Honrath, R. E., M. C. Peterson, M. P. Dziobak, J. E. Dibb, M. A. Arsenault, and S. A. Green (2000), Release of NO_x from sunlight-irradiated midlatitude snow, *Geophys. Res. Lett.*, *27*, 2237–2240, doi:10.1029/1999GL011286.
Hopper, J. F., B. Peters, Y. Yokouchi, H. Niki, B. T. Jobson, P. B. Shepson, and K. Muthuramu (1994), Chemical and meteorological observations at ice camp swan during polar sunrise experiment 1992, *J. Geophys. Res.*, *99*, 25,489–25,498, doi:10.1029/94JD02303.
Hopper, J. F., L. A. Barrie, A. Silis, W. Hart, A. J. Gallant, and H. Dryfhout (1998), Ozone and meteorology during the 1994 Polar Sunrise Experiment, *J. Geophys. Res.*, *103*, 1481–1492, doi:10.1029/97JD02888.
Huff, D. M., P. L. Joyce, G. J. Fochesatto, and W. R. Simpson (2011), Deposition of dinitrogen pentoxide, N_2O_5, to the snowpack at high latitudes, *Atmos. Chem. Phys.*, *11*, 4929–4938.
Ianniello, A., H. J. Beine, R. Sparapani, F. Di Bari, I. Allegrini, and J. D. Fuentes (2002), Denuder measurements of gas and aerosol species above Arctic snow surfaces at Alert 2000, *Atmos. Environ.*, *36*, 5299–5309.
Ianniello, A., H. J. Beine, M. S. Landis, R. K. Stevens, G. Esposito, A. Arnoroso, and I. Allegrini (2007), Comparing field performances of denuder techniques in the high Arctic, *Atmos. Environ.*, *41*, 1604–1615.
Ianniello, A., F. Spataro, G. Esposito, I. Allegrini, M. Hu, and T. Zhu (2011), Chemical characteristics of inorganic ammonium salts in PM2.5 in the atmosphere of Beijing (China), *Atmos. Chem. Phys.*, *11*, 10,803–10,822.
Jacobi, H. W., and B. Hilker (2007), A mechanism for the photochemical transformation of nitrate in snow, *J. Photochem. Photobiol., A*, *185*, 371–382.
Jacobi, H. W., S. Morin, and J. W. Bottenheim (2010), Observation of widespread depletion of ozone in the springtime boundary layer of the central Arctic linked to mesoscale synoptic conditions, *J. Geophys. Res.*, *115*, D17302, doi:10.1029/2010JD013940.
Jacobi, H. W., J. Kleffmann, G. Villena, P. Wiesen, M. King, J. France, C. Anastasio, and R. Staebler (2014), Role of Nitrate in the Photochemical Formation of Radicals in the Snow, *Environ. Sci. Technol.*, *48*, 165–172.
Jarvis, J. C., E. J. Steig, M. G. Hastings, and S. A. Kunasek (2008), Influence of local photochemistry on isotopes of nitrate in Greenland snow, *Geophys. Res. Lett.*, *35*, L21804, doi:10.1029/2008GL035551.
Jarvis, J. C., M. G. Hastings, E. J. Steig, and S. A. Kunasek (2009), Isotopic ratios in gas-phase HNO_3 and snow nitrate at Summit, Greenland, *J. Geophys. Res.*, *114*, D17301, doi:10.1029/2009JD012134.

Johansson, C., and L. Granat (1986), An experimental-study of the dry deposition of gaseous nitric-acid to snow, *Atmos. Environ.*, *20*, 1165–1170.

Jones, A. E., R. Weller, E. W. Wolff, and H. W. Jacobi (2000), Speciation and rate of photochemical NO and NO_2 production in Antarctic snow, *Geophys. Res. Lett.*, *27*, 345–348, doi:10.1029/1999GL010885.

Jones, A. E., R. Weller, P. S. Anderson, H. W. Jacobi, E. W. Wolff, O. Schrems, and H. Miller (2001), Measurements of NO_x emissions from the Antarctic snowpack, *Geophys. Res. Lett.*, *28*, 1499–1502, doi:10.1029/2000GL011956.

Kaiser, J., M. G. Hastings, B. Z. Houlton, T. Rockmann, and D. M. Sigman (2007), Triple oxygen isotope analysis of nitrate using the denitrifier method and thermal decomposition of N_2O, *Anal. Chem.*, *79*, 599–607.

Kendall, C. (1998), Tracing nitrogen sources and cycling in catchments, in *Isotope Tracers in Catchment Hydrology*, edited by C. Kendall and J. J. McDonnell, 839 pp., Elsevier Sci., Amsterdam.

Kendall, C., E. M. Elliott, and S. D. Wankel (2007), Tracing anthropogenic inputs of nitrogen to ecosystems, in *Stable Isotopes in Ecology and Environmental Science*, edited by R. H. Michener and K. Lajtha, pp. 375–449, Blackwell, Malden, Mass.

Kuhn, M. (2001), The nutrient cycle through snow and ice, a review, *Aquat. Sci.*, *63*, 150–167.

Kühnel, R. (2013), *Reactive Nitrogen: Transport to and Deposition at the High Arctic site Ny-Ålesund, Svalbard*, 236 pp., Univ. of Oslo, Oslo.

Kühnel, R., T. J. Roberts, M. P. Björkman, E. Isaksson, W. Aas, K. Holmén, and J. Ström (2011), 20-Year Climatology of NO_3^- and NH_4^+ Wet Deposition at Ny-Ålesund, Svalbard, *Adv. Meteorol.*, *2011*, 10.

Kvlividz, V. I., V. F. Kiselev, and L. A. Ushakova (1970), Existence of Quasi-Liquid Layer on Ice Surface [in Russian], *Doklady Akademii Nauk Sssr*, *191*, 1088–1090.

Larose, C., S. Berger, C. Ferrari, E. Navarro, A. Dommergue, D. Schneider, and T. M. Vogel (2010), Microbial sequences retrieved from environmental samples from seasonal Arctic snow and meltwater from Svalbard, Norway, *Extremophiles*, *14*, 205–212.

Ma, W. K., A. Schautz, L. A. E. Fishback, A. Bedard-Haughn, R. E. Farrell, and S. D. Siciliano (2007), Assessing the potential of ammonia oxidizing bacteria to produce nitrous oxide in soils of a high arctic lowland ecosystem on Devon Island, Canada, *Soil Biol. Biochem.*, *39*, 2001–2013.

McCabe, J. R., C. S. Boxe, A. J. Colussi, M. R. Hoffmann, and M. H. Thiemens (2005), Oxygen isotopic fractionation in the photochemistry of nitrate in water and ice, *J. Geophys. Res.*, *110*, D15310, doi:10.1029/2004JD005484.

Michalski, G., Z. Scott, M. Kabiling, and M. H. Thiemens (2003), First measurements and modeling of $\Delta^{17}O$ in atmospheric nitrate, *Geophys. Res. Lett.*, *30*(16), 1870, doi:10.1029/2003GL017015.

Miteva, V. (2008), *Bacteria in Snow and Glacier Ice*, pp. 31–50, Springer, Berlin.

Morin, S., J. Savarino, S. Bekki, A. Cavender, P. B. Shepson, and J. W. Bottenheim (2007a), Major influence of BrO on the NO_x and nitrate budgets in the Arctic spring, inferred from $\Delta^{17}O(NO_3^-)$ measurements during ozone depletion events, *Environ. Chem.*, *4*, 238–241.

Morin, S., J. Savarino, S. Bekki, S. Gong, and J. W. Bottenheim (2007b), Signature of Arctic surface ozone depletion events in the isotope anomaly (Delta O-17) of atmospheric nitrate, *Atmos. Chem. Phys.*, *7*, 1451–1469.

Morin, S., J. Savarino, M. M. Frey, N. Yan, S. Bekki, J. W. Bottenheim, and J. M. F. Martins (2008), Tracing the origin and fate of NO_x in the Arctic atmosphere using stable isotopes in nitrate, *Science*, *322*, 730–732.

Morin, S., J. Savarino, M. M. Frey, F. Domine, H. W. Jacobi, L. Kaleschke, and J. M. F. Martins (2009), Comprehensive isotopic composition of atmospheric nitrate in the Atlantic Ocean boundary layer from 65 degrees S to 79 degrees N, *J. Geophys. Res.*, *114*, D05303, doi:10.1029/2008JD010696.

Perrino, C., D. Ramirez, and I. Allegrini (2001), Monitoring acidic air pollutants near Rome by means of diffusion lines: Development of a specific quality control procedure, *Atmos. Environ.*, *35*, 331–341.

Qiu, R., S. A. Green, R. E. Honrath, M. C. Peterson, Y. Lu, and M. Dziobak (2002), Measurements of J_{NO3^-} in snow by nitrate-based actinometry, *Atmos. Environ.*, *36*, 2563–2571.

Rahn, K. A. (1981), Relative importances of North-America and Eurasia as sources of Arctic aerosol, *Atmos. Environ.*, *15*, 1447–1455.

Rahn, K. A., E. Joranger, A. Semb, and T. J. Conway (1980), High winter concentrations of SO_2 in the Norwegian Arctic and transport from Eurasia, *Nature*, *287*, 824–826.

Roberts, T. J., A. Hodson, C. D. Evans, and K. Holmén (2010), Modelling the impacts of a nitrogen pollution event on the biogeochemistry of an Arctic glacier, *Ann. Glaciol.*, *51*, 163–170.

Russell, A. G., G. J. Mcrae, and G. R. Cass (1985), The dynamics of nitric-acid production and the fate of nitrogen-oxides, *Atmos. Environ.*, *19*, 893–903.

Sander, R., and J. Bottenheim (2012), A compilation of tropospheric measurements of gas-phase and aerosol chemistry in polar regions, *Earth Syst. Sci. Data*, *4*, 215–282.

Sato, K., N. Takenaka, H. Bandow, and Y. Maeda (2008), Evaporation loss of dissolved volatile substances from ice surfaces, *J. Phys. Chem. A*, *112*, 7600–7607.

Seinfeld, J. H., and S. N. Pandis (2006), *Atmosperic Chemistry and Physics: From Air Pollution to Climate Change*, 2nd ed., John Wiley, Hoboken, N. J.

Siciliano, S. D., W. K. Ma, S. Ferguson, and R. E. Farrell (2009), Nitrifier dominance of Arctic soil nitrous oxide emissions arises due to fungal competition with denitrifiers for nitrate, *Soil Biol. Biochem.*, *41*, 1104–1110.

Sigman, D. M., K. L. Casciotti, M. Andreani, C. Barford, M. Galanter, and J. K. Bohlke (2001), A bacterial method for the nitrogen isotopic analysis of nitrate in seawater and freshwater, *Anal. Chem.*, *73*, 4145–4153.

Simpson, W. R., M. D. King, H. J. Beine, R. E. Honrath, and X. L. Zhou (2002), Radiation-transfer modeling of snow-pack photochemical processes during ALERT 2000, *Atmos. Environ.*, *36*, 2663–2670.

Simpson, W. R., et al. (2007), Halogens and their role in polar boundary-layer ozone depletion, *Atmos. Chem. Phys.*, *7*, 4375–4418.

Sozzi, R., M. Favaron, and T. Georgiadis (1998), Method for estimation of surface roughness and similarity function of wind speed vertical profile, *J. Appl. Meteorol.*, *37*, 461–469.

Spataro, F., A. Ianniello, G. Esposito, I. Allegrini, T. Zhu, and M. Hu (2013), Occurrence of atmospheric nitrous acid in the urban area of Beijing (China), *Sci. Total Environ.*, *447*, 210–224.

Stohl, A. (2006), Characteristics of atmospheric transport into the Arctic troposphere. *J. Geophys. Res.*, *111*, D11306, doi:10.1029/2005JD006888.

Sturm, M., and J. B. Johnson (1991), Natural-convection in the sub-Arctic snow cover, *J. Geophys. Res.*, *96*, 11,657–11,671, doi:10.1029/91JB00895.

Thomas, J. L., J. Stutz, B. Lefer, L. G. Huey, K. Toyota, J. E. Dibb, and R. von Glasow (2011), Modeling chemistry in and above snow at Summit, Greenland—Part 1: Model description and results, *Atmos. Chem. Phys.*, *11*, 4899–4914.

Thomas, J. L., J. E. Dibb, L. G. Huey, J. Liao, D. Tanner, B. Lefer, R. von Glasow, and J. Stutz (2012), Modeling chemistry in and above snow at Summit, Greenland—Part 2: Impact of snowpack chemistry on the oxidation capacity of the boundary layer, *Atmos. Chem. Phys.*, *12*, 6537–6554.

Vega, C. P. (2014), *Nitrate Stable Isotopes and Major Ions in Snow and Ice From Svalbard*, 80 pp., Uppsala Univ., Uppsala, Sweden.

Villena, G., et al. (2011), Nitrous acid (HONO) during polar spring in Barrow, Alaska: A net source of OH radicals?, *J. Geophys. Res.*, *116*, D00R07, doi:10.1029/2011JD016643.

Zhou, X. L., H. J. Beine, R. E. Honrath, J. D. Fuentes, W. Simpson, P. B. Shepson, and J. W. Bottenheim (2001), Snowpack photochemical production of HONO: A major source of OH in the Arctic boundary layer in springtime, *Geophys. Res. Lett.*, *28*, 4087–4090, doi:10.1029/2001GL013531.

Zien, A. W., A. Richter, A. Hilboll, A.-M. Blechschmidt, and J. P. Burrows (2014), Systematic analysis of tropospheric NO_2 long-range transport events detected in GOME-2 satellite data, *Atmos. Chem. Phys.*, *14*, 7367–7396.